The Monogenic Wavelet Transform

Sofia C. Olhede and Georgios Metikas

***Abstract*—This paper extends the 1-D analytic wavelet transform to the 2-D monogenic wavelet transform. The transformation requires care in its specification to ensure suitable transform coefficients are calculated, and it is constructed so that the wavelet transform may be considered as both local and monogenic. This is consistent with defining the transform as a real wavelet transform of a monogenic signal in analogy with the analytic wavelet transform. Classes of monogenic wavelets are proposed with suitable local properties. It is shown that the monogenic wavelet annihilates anti-monogenic signals, that the monogenic wavelet transform is phase-shift covariant and that the transform magnitude is phase-shift invariant. A simple form for the magnitude and orientation of the isotropic transform coefficients of a unidirectional signal when observed in a rotated frame of reference is derived. The monogenic wavelet ridges of local plane waves are given.**

***Index Terms*—Analytic signal, analytic wavelet transform, Hilbert transform, monogenic signal, Riesz transform.**

I. Introduction

THE analytic wavelet transform (AWT) is an important tool for 1-D signal processing. Its utility is based on a number of useful properties; for example its magnitude will not oscillate around singularities as the transform magnitude is locally nearly shift invariant [1]. Attention has focused on approximating the transform using finite length filters [2]–[4], and the continuous transform has been used to characterize oscillations and discontinuities [5]–[8]. The key to understanding the AWT is via its phase and magnitude. Local variation in the signal is mainly described by the phase, with the magnitude of the coefficients varying smoothly, this producing transform stability [3]. The AWT can be thought of as the combination of two operations, "localization" in time-frequency and "analytization," or how to restrict a function in time and frequency and simultaneously construct an analytic signal.

This paper focuses on the formal extension of the 1-D AWT into the 2-D monogenic wavelet transform (MWT). In 2-D, the definition of an analytic signal, or a hyperanalytic signal, is ambiguous. Popular definitions include the *monogenic signal* [9]–[12] and the *hypercomplex signal*; see [13]. One important characteristic of the 1-D analytic signal is that when evaluated in a complex argument it satisfies the Cauchy–Riemann equations in the upper half plane [14, p. 5–6]. In this paper a general definition is given for a *hyperanalytic signal* in arbitrary dimensions as the limit of a function satisfying an appropriate generalization of the Cauchy–Riemann equations. To justify using the Riesz system (or the monogenic signal), we discuss the analysis of 1-D structure embedded in 2-D. We represent the monogenic signal using its polar representation [11] and quaternions.

In 2-D, local misalignment can be represented by rotations and shifts of the argument of a signal. The extension of the phase-shift and small spatial shift invariance of the magnitude in 1-D should therefore be extended to such motion in 2-D. We discuss the decomposition of a real-valued image into a sum of a monogenic and an anti-monogenic signal in direct analogue with the orthogonal sum of square integrable 1-D functions into the two Hardy spaces [15, p. 10], of analytic and anti-analytic signals. This decomposition is fundamental for determining local relationships between signals and transform stability.

We need to combine the monogenic signal with the act of localization. To this purpose we define general quaternionic (vector-valued) mother wavelet functions, and a quaternionic wavelet family; see Section IV-A. Two special important cases are treated, namely starting from an isotropic real-valued mother wavelet, or from a directional real-valued mother wavelet. Special cases of families of wavelet functions are defined using for example the Morse wavelet families; see [7] and [16]–[18].

The quaternionic wavelet transform is defined in Section V. We discuss the symmetry properties of the quaternionic coefficients as compared to real-valued wavelet coefficients. These properties are important for the understanding of phase. We define the MWT and derive its properties in Section V-B. We determine that the interpretation of the MWT coefficients is in every way consistent with a jointly local and monogenic representation of a signal, in Proposition 3. The MWT, corresponding to a quaternionic object, is represented by its magnitude, phase and orientation. We demonstrate how the MWT annihilates the rotated anti-monogenic component of the signal, this establishing the interpretation of the phase of the MWT coefficients. We note the form of the MWT of a plane wave, and the MWT ridges.

We note that the magnitude of the isotropic MWT is invariant to local rotations. For locally unidirectional signals the orientation of a signal may be determined directly from the isotropic MWT. This gives the justification for decomposing a locally directional signal only in scale, location and monogenic components. We consider the effect of local phase-shifts of the signal. We show that for locally orientationally stable signals, shifts in phase are represented only by the phase of the wavelet coefficients. The magnitudes of the wavelet coefficients are stable and locally shift-invariant; see Theorem 4. This establishes an analogue of the approximate shift-invariance observed for the AWT; see [1, p. 143].

Manuscript received June 10, 2008; accepted April 23, 2009. First published May 19, 2009; current version published August 12, 2009. The associate editor coordinating the review of this manuscript and approving it for publication was Prof. Haldun M. Ozaktas. This work was supported by an EPSRC Grant GR/S64059/01.

S. C. Olhede is with the Department of Statistical Science, University College London, WC1E 6BT, London, U.K. (e-mail: s.olhede@ucl.ac.uk).

G. Metikas is with the Deutsche Bank, EC2N 2DB, London, U.K. (e-mail: gmet333@hotmail.com).

Digital Object Identifier 10.1109/TSP.2009.2023397

The MWT as introduced in this article is not without precursors. Cnops [19] introduced a version of the isotropic MWT while Metikas and Olhede [17] discussed the localization of the isotropic Morse wavelets, and their usage. Unser *et al.* [20] have introduced discrete wavelets for calculating the isotropic MWT, establishing discrete results analogously to [17]. Brackx and coworkers [21], [22] investigated special families of wavelets, the Clifford wavelet families. Other work on quaternionic decompositions of note are [23]–[28]. Most of the latter contributions correspond to constructing local versions of a quaternionic Fourier Transform. Utilizing phase structure of complex wavelet coefficients for denoising is treated in [29] and [30]. Note also work by Hsieh [31] (motion smoothing) and He and Yu [32]. Duits *et al.* [33] have developed oriented signal representations based on *orientation scores*. Wavelet theory is in this work extended to representing 2-D images in a directional representation *without* including a full range of scales. This leads to a substantial saving in terms of storage requirements. Frequently images contain variability in many orientations associated with different components and the MWT complements the orientation score, as the scale localization allows us to isolate individual components and represent their directionality using the monogenic components without a high-resolution decomposition in orientation. The name "monogenic wavelet" has been utilized before in a different context [34].

In contrast to the aforementioned results this paper defines the generic monogenic continuous wavelet transform, determines the properties of monogenic wavelets, and their transform coefficients. The interpretation of the coefficients is established to justify the choice of definition of the MWT. The concepts of transform phase and magnitude are clarified. The introduction of the decomposition of a real-valued signal into its monogenic and anti-monogenic components is a necessary development for these results. A version of the MWT has already been used for denoising [35] and for nonstationary plane-wave estimation [17], [36]. Given the suitable theoretical properties of the continuous MWT, appropriate discretized versions, such as [20], are of great importance, and lead the way for future innovation.

Notation

We let AWT abbreviate the analytic wavelet transform, CWT is the continuous wavelet transform, FT is the Fourier transform, HT is the Hilbert transform [14], MWT is the monogenic wavelet transform, QFT is the quaternion Fourier transform [37], RT is the Riesz transform, and UQFT is the unit quaternion Fourier transform [37]. $*$ and $**$ are the 1-D and 2-D convolution operations. $\mathbf{x}$ is used as the spatial variable, $\mathbf{f}$ as the frequency variable, and $\mathbf{q}$ as the quaternionic frequency variable. Their moduli are $x = ||\mathbf{x}||$, $f = ||\mathbf{f}||$ and $q = ||\mathbf{q}||$. We take $\phi = \tan^{-1}(f_2/f_1), \eta = \tan^{-1}(q_2/q_1), \chi = \tan^{-1}(x_2/x_1)$ $\phi_b = \tan^{-1}(f_{b,2}/f_{b,1}), \eta_b = \tan^{-1}(q_{b,2}/q_{b,1})$ and $\chi_b = \tan^{-1}(b_2/b_1)$. We let $\mathcal{T}_{\mathbf{b}}\{g(\mathbf{x})\} = g(\mathbf{x}-\mathbf{b})$ be the translation operator, $\mathcal{D}_a\{g(\mathbf{x})\} = a^{-1}g(\mathbf{x}/a)$ be the dilation operator, $R_\theta g(\mathbf{x}) = g(\mathbf{R}_{-\theta}\mathbf{x})$ be the rotation operator, for $\theta \in [0, 2\pi)$, and $\mathcal{J}_\theta\{g(\mathbf{x})\} = g(\mathbf{J}_\theta\mathbf{x})$ be the reflection operator. $\mathbf{R}_\theta = ((\cos(\theta) - \sin(\theta)), (\sin(\theta)\ \cos(\theta)))$ and $\mathbf{J}_\theta = ((\cos(2\theta)\ \sin(2\theta))\ (\sin(2\theta) - \cos(2\theta)))$. An arbitrary quaternion [38] takes the form $e = e_1 + e_2\boldsymbol{i} + e_3\boldsymbol{j} + e_4\boldsymbol{k} \in \mathbb{H}$ where $e_l \in \mathbb{R}$, $l = 1, \ldots 4$, and $\mathbb{H}$ is the four-dimensional real associative algebra of the quaternions. We note that: $\boldsymbol{i}^2 = \boldsymbol{j}^2 = \boldsymbol{k}^2 = \boldsymbol{ijk} = -1$, while $\boldsymbol{ij} = -\boldsymbol{ji} = \boldsymbol{k}$, $\boldsymbol{ik} = -\boldsymbol{ki} = -\boldsymbol{j}$, and $\boldsymbol{jk} = -\boldsymbol{kj} = \boldsymbol{i}$. e has conjugate $e^* = e_1 - e_2\boldsymbol{i} - e_3\boldsymbol{j} - e_4\boldsymbol{k}$, and e can be written as $e = \Re\{e\} + \mathsf{P}u\{e\}$, where $\Re\{e\} = 1/2\,(e + e^*)$, is the real part and $\mathsf{P}u\{e\} = 1/2\,(e - e^*)$, is a pure quaternion. A pure unit quaternion is written as $\boldsymbol{e} = 0 + \boldsymbol{i}e_2 + \boldsymbol{j}e_3 + \boldsymbol{k}e_4$, where $\sum_{j=2}^{4} e_j^2 = 1$ and a pure unit quaternion without $\boldsymbol{k}$ component as $\boldsymbol{e}_\nu = \cos(\nu)\boldsymbol{i} + \sin(\nu)\boldsymbol{j}$.

II. Phase, Lower Dimensional Structure and Analyticity

A. Analyticity and Hyperanalyticity

The monogenic signal is a generalization of the analytic signal [14]. In 1-D the instantaneous frequency and amplitude of a signal are defined from the analytic signal [39]. Such a representation is suitable for a 1-D oscillatory signal, $c(x_1) = a_c(x_1)\cos(2\pi\varphi_c(x_1)) = \Re\left\{a_c(x_1)e^{2\pi\boldsymbol{j}\varphi_c(x_1)}\right\}$, where $a_c(x_1)$ is the amplitude and $\varphi_c(x_1)$ is the phase. We use the definition of the FT of a d-dimensional signal $g(\mathbf{x})$ of

$$G(\mathbf{f}) = \mathcal{F}\{g\}(\mathbf{f}) = \int_{\mathbb{R}^d} g(\mathbf{x})e^{-2\boldsymbol{j}\pi\mathbf{f}^T\mathbf{x}}\,d\mathbf{x}$$
$$g(\mathbf{x}) = \int_{\mathbb{R}^d} |G(\mathbf{f})|\,e^{2\boldsymbol{j}\pi(\mathbf{f}^T\mathbf{x} - \Phi_g(\mathbf{f}))}\,d\mathbf{f} \tag{1}$$

where $G(\mathbf{f}) = |G(\mathbf{f})|\,e^{-2\boldsymbol{j}\pi\Phi_g(\mathbf{f})}$, with $\Phi_g(\mathbf{f})$ as the phase of the FT. The analytic signal is then $g^+(x_1) = 2\int_0^\infty G(f)e^{2\pi\boldsymbol{j}fx_1}\,df = g(x_1) + \boldsymbol{j}g^{(1)}(x_1)$, with $g^{(1)}(x_1)$ the HT of $g(x_1)$, defined [14] by

$$g^{(1)}(x_1) = \mathcal{H}\{g\}(x_1) = \frac{1}{\pi}\fint_{-\infty}^{\infty} \frac{g(y)}{x_1 - y}\,dy$$
$$G^+(f_1) = G(f_1)\,(1 + \operatorname{sgn}(f_1)) \tag{2}$$

using a principal value integral and $G^+(f_1)$ corresponds to the FT of the analytic signal. The anti-analytic signal is defined as $g^-(x_1) = g(x_1) - \boldsymbol{j}g^{(1)}(x_1)$. If the FT of $e^{2\pi\boldsymbol{j}\varphi_c(x_1)}$ is only supported at frequencies higher than those at which the FT of $a_c(x_1)$ are supported, then we can retrieve the true phase and amplitude of $c(x_1)$ from the phase and amplitude of $c^+(x_1)$[14, p. 88–90] (Bedrosian's Theorem). This is the motivation for representing a generic signal $g(x_1)$ via its local amplitude and phase. These two functions may then be defined from $a_g(x_1) = |g^+(x_1)|$, and $\varphi_g(x_1) = 1/(2\pi)\tan^{-1}\left(g^{(1)}(x_1)/g(x_1)\right)$.

The 1-D analytic signal is the limit of an analytic function, satisfying the Cauchy–Riemann equations in the upper half of the complex plane [14, p. 5–6]. Note that an analytic signal evaluated in a complex-valued argument is still an analytic function. The decomposition of real-valued $g(x_1) \in L^2(\mathbb{R})$ into two complex-valued analytic and anti-analytic functions , $g^+(x_1)$ and $g^-(x_1)$ respectively, of

$$g(x_1) = \frac{1}{2}\left(g^+(x_1) + g^-(x_1)\right) \tag{3}$$

corresponds to the analytic decomposition of $g(x_1)$ [40]. The analytic decomposition is important for deriving the properties of the 1-D analytic wavelet transform, as shown in [41, p. 426], due to the fact that the analytic wavelet annihilates the

anti-analytic component in the decomposition. The analytic and anti-analytic signals are represented in polar form by $g^{\pm}(x_1) = |g^{\pm}(x_1)|\, e^{\pm 2\pi \boldsymbol{j}\varphi_g(x_1)}$, where we interpret $|g^{\pm}(x_1)|^2$ as the local energy and $\varphi_g(x_1)$, as the local structural representation of $g(x_1)$. Starting from the analytic decomposition we obtain an oscillatory representation of $g(x_1)$ by

$$\begin{aligned} g(x_1) &= \frac{1}{2}\left(g(x_1)+\boldsymbol{j}g^{(1)}(x_1)+g(x_1)-\boldsymbol{j}g^{(1)}(x_1)\right) \\ &= a_g(x_1)\cos(2\pi\varphi_g(x_1)). \end{aligned} \tag{4}$$

Thus, a local magnitude $a_g(x_1)$ and phase $\varphi_g(x_1)$ can for any real-valued function $g(x_1)$ be defined from the modulus and phase of $g^{\pm}(x_1)$. In higher dimensions to determine analogues of $a_g(x_1)$ and $\varphi_g(x_1)$ from an observed real-valued function $g(\mathbf{x})$ the analogue or analogues of function $g^{(1)}(x_1)$ must be defined. To this purpose 2-D extensions of the Cauchy–Riemann equations are used, and any set of equations corresponding to extensions of these equations, is a set of *generalized Cauchy–Riemann equations*. We define the domain $\Gamma^{(p)}$ by $\Gamma^{(p)} = \{\mathbf{y},\, y_i > 0,\, i = 1, \ldots, p\}$.

Definition 3.1: The hyperanalytic function and signal.

Any vector-valued function $\mathbf{k}_g^+(\mathbf{x},\mathbf{y})$, in spatial variable $\mathbf{x}$, with associated p dimensional auxiliary variable $\mathbf{y}$, that satisfies a given 2-D generalization of the Cauchy–Riemann equations for $\mathbf{y} \in \Gamma^{(p)}$ is a *hyperanalytic function*. Any vector-valued function $g^+(\mathbf{x})$, that can be written as the limit as $\mathbf{y} \rightarrow \mathbf{0}^+$ of a hyperanalytic function $\mathbf{k}_g^+(\mathbf{x},\mathbf{y})$, is a *hyperanalytic signal*.

B. The Monogenic Signal

A popular choice of a 2-D generalization to the Cauchy–Riemann equations is given by the Riesz system [42]. The Cauchy–Riemann equations are given for functions in a complex variable $z = x + \boldsymbol{j}y$, while the 2-D Riesz system of equations is defined for the triplet of variables (x_1, x_2, y), and is satisfied by a three-vector valued function. Any solution of the Riesz system in the upper half-space ($y > 0$) is a *monogenic function* [43, p. 35]. Note that if $k^+(\mathbf{x}, y)$ is a monogenic function then $k^{+*}(\mathbf{x}, y)$ is a solution of the Riesz system in the lower half-space ($y < 0$), and will be referred to as an *anti-monogenic function*, with notation $k^-(\mathbf{x}, y)$. We define the Riesz kernels [42], [44] ($\{r_l\}$) and transform ($\mathcal{R}g$) by

$$\begin{aligned} r_l(\mathbf{x}) &= c_n \frac{x_l}{|\mathbf{x}|^3}, \quad R_l(\mathbf{f}) = -\boldsymbol{j}\frac{f_l}{f}, \\ R_{1,Q}(\mathbf{q}) &= -\boldsymbol{i}\frac{q_1}{q}, \\ R_{2,Q}(\mathbf{q}) &= -\boldsymbol{j}\frac{q_2}{q}, \quad l = 1, 2, \\ \mathcal{R}g(\mathbf{x}) &= \boldsymbol{i}\mathcal{R}_1 g(\mathbf{x}) + \boldsymbol{j}\mathcal{R}_2 g(\mathbf{x}), \\ \mathcal{R}_l g(\mathbf{x}) &= g^{(l)}(\mathbf{x}) = (r_l **g)(\mathbf{x}),\ l = 1, 2. \end{aligned} \tag{5, 6}$$

Recently introduced by Felsberg and Sommer [11] into image processing the *monogenic*, and *anti-monogenic signals* of real signal $g(\mathbf{x})$, are defined by applying operator $\mathcal{M}^{\pm}$ to signal $g(\mathbf{x})$ as

$$\begin{aligned} g^{\pm}(\mathbf{x}) &= \mathcal{M}^{\pm} g(\mathbf{x}) = g(\mathbf{x}) \pm \mathcal{R}g(\mathbf{x}) \\ &= g(\mathbf{x}) \pm \left(\boldsymbol{i}g^{(1)}(\mathbf{x}) + \boldsymbol{j}g^{(2)}(\mathbf{x})\right). \end{aligned} \tag{7}$$

Letting $y \rightarrow 0^+$ the monogenic signal is retrieved from the monogenic function [43, p. 36]. Signals are often not observed in axes of special importance. Intrinsic orientational structure must be recognized from data. To this purpose the rotated monogenic, and rotated anti-monogenic signals of $g(\mathbf{x})$ are defined

$$\begin{aligned} g_\theta^{\pm}(\mathbf{x}) &= R_\theta \mathcal{M}^{\pm} g(\mathbf{x}) = \mathcal{M}_\theta^{\pm} g(\mathbf{x}) \\ &= g(\mathbf{R}_{-\theta}\mathbf{x}) \pm (\boldsymbol{i}R_\theta\mathcal{R}_1 g(\mathbf{x}) + \boldsymbol{j}R_\theta\mathcal{R}_2 g(\mathbf{x})) \\ &= g(\mathbf{R}_{-\theta}\mathbf{x}) \pm \left(\boldsymbol{i}g^{(1)}(\mathbf{R}_{-\theta}\mathbf{x}) + \boldsymbol{j}g^{(2)}(\mathbf{R}_{-\theta}\mathbf{x})\right) \\ &= g_\theta(\mathbf{x}) \pm \left(\boldsymbol{i}g_\theta^{(1)}(\mathbf{x}) + \boldsymbol{j}g_\theta^{(2)}(\mathbf{x})\right) \end{aligned} \tag{8}$$

with $\theta \in [0, 2\pi)$, thus also defining $g_\theta^{(s)}(\mathbf{x})$ for $s = 1, 2$. The rotated monogenic signal with angle θ concurs with the rotated anti-monogenic signal for an angle taking the value $\theta + \pi$. It is still convenient to keep our definition for all $[0, 2\pi)$ rather than restricting the range of permitted values of θ. Also

$$\begin{aligned} \mathcal{F}\left\{g^{(1)}(\mathbf{R}_{-\theta}\mathbf{x})\right\} &= -\boldsymbol{j}\cos(\phi-\theta)G(\mathbf{R}_{-\theta}\mathbf{f}) \\ \mathcal{F}\left\{g^{(2)}(\mathbf{R}_{-\theta}\mathbf{x})\right\} &= -\boldsymbol{j}\sin(\phi-\theta)G(\mathbf{R}_{-\theta}\mathbf{f}). \end{aligned} \tag{9}$$

Furthermore, we may note that [recalling ϕ is the argument of $\mathbf{f}$, $\boldsymbol{ij} = \boldsymbol{k}$ and using (9) and (8)]:

$$G_\theta^{\pm}(\mathbf{f}) = \left(1 \pm \sin(\phi-\theta) \mp \boldsymbol{k}\cos(\phi-\theta)\right) G(\mathbf{R}_{-\theta}\mathbf{f}). \tag{10}$$

If the Fourier transform of any function $h(\mathbf{x})$, $H(\mathbf{f})$ say, can be written in the form of (10), where $G(\mathbf{f})$ is the FT of a real-valued signal, then it can be directly deduced that $H(\mathbf{f})$ corresponds to the rotated monogenic image of $g(\mathbf{x})$. Equation (10) can therefore be used to determine if a quaternionic object is a rotated monogenic signal, and what real-valued object plays the role of $g(\mathbf{x})$. If the signal is locally unidirectional then rotations are important to determining the simplest form of the signal. We define

$$\widetilde{g}_{-\theta}(\mathbf{x}) = g(\mathbf{R}_\theta\mathbf{x}) \tag{11}$$

$$\begin{aligned} \widetilde{g}_{-\theta,\theta}^{\pm}(\mathbf{x}) &= g(\mathbf{x}) \pm \left(\boldsymbol{i}\widetilde{g}_{-\theta}^{(1)}(\mathbf{R}_{-\theta}\mathbf{x}) + \boldsymbol{j}\widetilde{g}_{-\theta}^{(2)}(\mathbf{R}_{-\theta}\mathbf{x})\right) \\ \widetilde{g}_{-\theta}^{(l)}(\mathbf{x}) &= \mathcal{R}_l\widetilde{g}_{-\theta}(\mathbf{x}) \\ \mathcal{R}_1 R_{-\theta} g(\mathbf{x}) &= \cos(\theta)R_{-\theta}\mathcal{R}_1 g(\mathbf{x}) + \sin(\theta)R_{-\theta}\mathcal{R}_2 g(\mathbf{x}) \end{aligned} \tag{12}$$

the latter relation noted by [42, p. 241]. We may note from (11) that $\widetilde{g}_{-\theta}^{(1)}(\mathbf{R}_{-\theta}\mathbf{x}) \neq \mathcal{R}_1 g(\mathbf{x})$ and $\widetilde{g}_{-\theta}^{(2)}(\mathbf{R}_{-\theta}\mathbf{x}) \neq \mathcal{R}_2 g(\mathbf{x})$. Thus, the rotation operator, R_θ, and the RT operators, $\mathcal{R}_l$, $l = 1, 2$, do not commute, and so $\widetilde{g}_{-\theta,\theta}^{\pm}(\mathbf{x}) \neq g^{\pm}(\mathbf{x})$. The decomposition of real-valued $g(\mathbf{x}) \in L^2(\mathbb{R}^2)$ into two quaternionic components, $\widetilde{g}_{-\theta,\theta}^{+}(\mathbf{x})$ and $\widetilde{g}_{-\theta,\theta}^{-}(\mathbf{x})$, $g(\mathbf{x}) = 1/2\left(\widetilde{g}_{-\theta,\theta}^{+}(\mathbf{x}) + \widetilde{g}_{-\theta,\theta}^{-}(\mathbf{x})\right)$, is the (rotated) *monogenic decomposition* of $g(\mathbf{x})$, with

$$\widetilde{g}_{-\theta,\theta}^{\pm}(\mathbf{x}) = g(\mathbf{x}) \pm \left(\boldsymbol{i}\widetilde{g}_{-\theta}^{(1)}(\mathbf{R}_{-\theta}\mathbf{x}) + \boldsymbol{j}\widetilde{g}_{-\theta}^{(2)}(\mathbf{R}_{-\theta}\mathbf{x})\right).$$

The rotated monogenic signal is represented in terms of amplitude, phase and orientation by

$$g_\theta^{\pm}(\mathbf{x}) = |g_\theta^{+}(\mathbf{x})|\, e^{\pm 2\pi \boldsymbol{e}_{\nu_\theta}(\mathbf{x})\varphi_\theta(\mathbf{x})} \tag{13}$$

$$
\begin{aligned}
|g_\theta^+(\mathbf{x})| &= \sqrt{[g_\theta(\mathbf{x})]^2 + [g_\theta^{(1)}(\mathbf{x})]^2 + [g_\theta^{(2)}(\mathbf{x})]^2} \\
\boldsymbol{e}_{\nu_\theta}(\mathbf{x}) &= (\boldsymbol{i}\,\cos\nu_\theta(\mathbf{x}) + \boldsymbol{j}\,\sin\nu_\theta(\mathbf{x})) \\
\nu_\theta(\mathbf{x}) &= \tan^{-1}\left(\frac{g_\theta^{(2)}(\mathbf{x})}{g_\theta^{(1)}(\mathbf{x})}\right) \\
\varphi_\theta(\mathbf{x}) &= \frac{\tau_\theta(\mathbf{x})}{2\pi}\tan^{-1}\left(\frac{\sqrt{[g_\theta^{(1)}(\mathbf{x})]^2 + [g_\theta^{(2)}(\mathbf{x})]^2}}{g_\theta(\mathbf{x})}\right). \quad (14)
\end{aligned}
$$

$\tau_\theta(\mathbf{x}) = \operatorname{sgn}\left((\cos(\nu_\theta(\mathbf{x}))\ \sin(\nu_\theta(\mathbf{x})))^T(g_\theta^{(1)}(\mathbf{x})\ g_\theta^{(2)}(\mathbf{x}))\right)$. $\boldsymbol{e}_{\nu_\theta}(\mathbf{x})$ is a function of $\mathbf{x}$ as $\nu_\theta(\mathbf{x})$ is spatially varying. $\tau_\theta(\mathbf{x})$ is added to the definition of $\varphi_\theta(\mathbf{x})$ to enable $\varphi_\theta(\mathbf{x})$ to take values over a full range, namely $\varphi_\theta(\mathbf{x}) \in (-\pi, \pi]$ but $\nu_\theta(\mathbf{x}) \in [0, \pi]$. This way $\nu_\theta \in [0, \pi]$ defines an orientation (or axes of variation) and $\varphi_\theta(\mathbf{x})$ is supported over the full range of values $[-\pi, \pi)$, just like a 1-D phase function. If we analyze a quaternionic signal then it may be that the monogenic and anti-monogenic signals are not trivially related and the physical properties of the signal may prescribe signal monogenicity or signal anti-monogenicity, as is the case for the analyticity of complex-valued signals in applications; see [45].

The rotated polar representation of a real signal $g(\mathbf{x})$ (in terms of $\tilde{g}(\cdot)$) is given by $g(\mathbf{x}) = \Re\left\{\widetilde{g}^{\pm}_{-\theta,\theta}(\mathbf{x})\right\} = \left|\widetilde{g}^{\pm}_{-\theta,\theta}(\mathbf{x})\right|\cos(2\pi\widetilde{\varphi}_{-\theta,\theta}(\mathbf{x}))$. Locally a signal is described by its magnitude $\left|\widetilde{g}^{+}_{-\theta,\theta}(\mathbf{x})\right|$ and the local structure of the signal is determined by $\widetilde{\varphi}_{-\theta,\theta}(\mathbf{x})$, from which an instantaneous frequency is determined by $|\nabla\widetilde{\varphi}_{-\theta,\theta}(\mathbf{x})|$. It follows that $\left|\widetilde{g}^{\pm}_{-\theta,\theta}(\mathbf{x})\right| = |g^{\pm}(\mathbf{x})|$ (the magnitude at $\theta = 0$), $\widetilde{\varphi}_{-\theta,\theta}(\mathbf{x}) = \varphi(\mathbf{x})$ (the phase at $\theta = 0$), however $\boldsymbol{e}_{\widetilde{\nu}_{-\theta,\theta}}(\mathbf{x}) \neq \boldsymbol{e}_{\nu}(\mathbf{x})$ (the orientation at $\theta = 0$), but for convenience we shall write $\widetilde{\nu}(\mathbf{x})$ for $\widetilde{\nu}_{-\theta,\theta}(\mathbf{x})$. The monogenic representation of $g(\mathbf{x})$ is equivalent to the rotated monogenic representation, as only the orientation of the representation changes. The intuitive understanding of this is that the monogenic signal is constructing a plane wave representation of the signal at spatial point $\mathbf{x}$, where the orientation of the plane wave is determined from the signal. No matter what axes we use, the local plane wave representation in the amplitude and phase remain the same, but the parameterization of orientation changes. It is possible to define a new rotation operator ($\tilde{R}_\theta$, say) of a monogenic signal so that the target of the Riesz transforms is co-rotated with the argument of the signal

$$
\begin{aligned}
\tilde{R}_\theta\mathcal{M}^{\pm}g(\mathbf{x}) &= R_\theta g(\mathbf{x}) \pm (\boldsymbol{i} \quad \boldsymbol{j})\,\mathbf{R}_\theta\begin{pmatrix} R_\theta\mathcal{R}_1 g(\mathbf{x}) \\ R_\theta\mathcal{R}_2 g(\mathbf{x})\end{pmatrix} \\
&= R_\theta g(\mathbf{x}) \pm (\boldsymbol{i}\mathcal{R}_1 R_\theta g(\mathbf{x}) + \boldsymbol{j}\mathcal{R}_2 R_\theta g(\mathbf{x}))
\end{aligned}
$$

and thus $\tilde{R}_\theta\mathcal{M}^{\pm}\tilde{g}_{-\theta}(\mathbf{x}) = g(\mathbf{x}) \pm (\boldsymbol{i}\mathcal{R}_1 g(\mathbf{x}) + \boldsymbol{j}\mathcal{R}_2 g(\mathbf{x}))$.[1] While working out very neatly for the Riesz transforms such definitions of rotations do not make sense for *arbitrary* quaternion-valued functions. In fact if we have a pair of kernels, $g_1(\mathbf{x})$ and $g_2(\mathbf{x})$ say, that commute with translations and dilations and whose convolution with a signal correspond to bounded transformations on $L^2(\mathbb{R})$, then $g_1(\mathbf{x})$ and $g_2(\mathbf{x})$ *have to be* constant multiples of Riesz transforms [46, Prop. 2], for such simple rotation relationships to hold. The fact that $\tilde{R}_\theta\mathcal{M}^{\pm}\tilde{g}_{-\theta}(\mathbf{x})$ yields $g(\mathbf{x}) \pm (\boldsymbol{i}\mathcal{R}_1 g(\mathbf{x}) + \boldsymbol{j}\mathcal{R}_2 g(\mathbf{x}))$ implies that the monogenic wavelets will have a number of suitable rotation properties.

Exploiting the Hermitian symmetry of the FT of a real image $G^*(\mathbf{f}) = G(-\mathbf{f})$, we have

$$
\begin{aligned}
\langle g^{(1)}, g\rangle &= \int d\mathbf{f}\ \boldsymbol{j}\,\frac{f_1}{f}\,G^*(\mathbf{f})\,G(\mathbf{f}) \\
&= \int d\mathbf{f}\ \boldsymbol{j}\,\frac{f_1}{f}\,G(-\mathbf{f})\,G(\mathbf{f}) = 0. \quad (15)
\end{aligned}
$$

This is a direct generalization of the $n = 1$ case where $\langle g^{(1)}, g\rangle = 0$. However, $g^{(1)}(\mathbf{x})$ and $g^{(2)}(\mathbf{x})$ do not always satisfy $\langle g^{(1)}, g^{(2)}\rangle = 0$. Such relationships are important for determining the statistical properties of the RT, as well as the localized RT; see also [17] and [35], as deriving the distribution of noisy monogenic coefficients requires determining the covariance between the components of a three-vector of $\boldsymbol{g}(\mathbf{x}) = \left(g(\mathbf{x})\ g^{(1)}(\mathbf{x})\ g^{(2)}(\mathbf{x})\right)$. If the signal $g(\mathbf{x})$ is also radially symmetric, then it also follows $\langle g^{(2)}, g^{(1)}\rangle = 0$. The norm of the Riesz components is given by (as noted by [11, p. 3140]):

$$
\begin{aligned}
\langle g^{(s)}, g^{(s)}\rangle &= \int \frac{f_s^2}{f^2} G(-\mathbf{f})G(\mathbf{f})d\mathbf{f},\ s = 1, 2 \\
\langle g^{(1)}, g^{(1)}\rangle &+ \langle g^{(2)}, g^{(2)}\rangle = \langle g, g\rangle. \quad (16)
\end{aligned}
$$

If furthermore $g(\mathbf{x})$ is radially symmetric then $\langle g^{(s)}, g^{(s)}\rangle = 1/2\langle g, g\rangle$, $s = 1, 2$. These relationships were used in [17] in the special case of the isotropic multiple Morse wavelets, and special forms were also derived for the discrete wavelet transform of a monogenic signal [35].

C. Unidirectional Signals and Fourier Descriptions

Wavelets are spatially localized functions associated with a certain period or periods. In 2-D we may use other frequency-domain descriptions than the regular FT; see Pei *et al.* [37] or Bülow *et al.* [47]. The unit quaternion Fourier transform (UQFT) [37] in an arbitrary pure unit quaternion $\boldsymbol{e}$ is

$$
\begin{aligned}
G_{\boldsymbol{e}}(\mathbf{f}) &= \mathcal{F}_{\boldsymbol{e}}\{g\}(\mathbf{f}) = \int_{-\infty}^{\infty}\int_{-\infty}^{\infty} g(\mathbf{x})e^{-2\pi\boldsymbol{e}\mathbf{f}^T\mathbf{x}}\,d\mathbf{x} \\
g(\mathbf{x}) &= \int_{-\infty}^{\infty}\int_{-\infty}^{\infty} G_{\boldsymbol{e}}(\mathbf{f})e^{2\pi\boldsymbol{e}\mathbf{f}^T\mathbf{x}}\,d\mathbf{f}. \quad (17)
\end{aligned}
$$

The transform is also known as the Type 3 QFT; see Pei *et al.* [37, p. 2784]. The UQFT is still interpretable as a sinusoidal decomposition of structure, as any pure unit $\boldsymbol{e}$ satisfies the De Moivre's relationships.

A unidirectional signal, $g_U(\mathbf{x})$ say, can for some given $\mathbf{n} = (\cos(\nu)\ \sin(\nu))$, with $\nu \in [0, \pi)$, be modelled as $g_U(\mathbf{x}) = \int_0^\infty G_U(f)\cos(2\pi f\mathbf{n}^T\mathbf{x})\ df$[35, p. 1525]. The monogenic signal of $g_U(\mathbf{x})$ is

$$
\begin{aligned}
g_U^+(\mathbf{x}) &= \int_0^\infty G_U(f)\cos(2\pi f\mathbf{n}^T\mathbf{x})df \\
&\quad + \boldsymbol{e}_\nu\int_0^\infty G_U(f)\sin(2\pi f\mathbf{n}^T\mathbf{x})df. \quad (18)
\end{aligned}
$$

[1]The authors gratefully acknowledge a referee for proposing this rotation operator and noting the form of $\tilde{R}_\theta\mathcal{M}^{\pm}\tilde{g}_{-\theta}$.

This follows by exchanging the order of the MT and the integral, and then using the expression for the monogenic extension of a sinusoid given in [11], recalling the definition of $\mathbf{n}$. The global orientation of the globally directional signal in this case may be determined from the monogenic signal by calculating the arctangent of the ratio of the two RTs. It may be shown, again using the monogenic extension of a sinusoid given in [11], that $G^{+}_{U,\boldsymbol{e}_\nu}(\mathbf{f}) = G_U(f),\ f > 0$ and $G^{+}_{U,\boldsymbol{e}_\nu}(\mathbf{f}) = 0,\ f < 0$. Thus, the spectral support of the UQFT of the signal in $\boldsymbol{e}_\nu$ is one-sided, and limited to the positive frequencies, just like a 1-D analytic signal. The result is to be expected, as a plane wave is really a 1-D feature.

If the signal corresponds to unidirectional variation only, the monogenic signal is extracting the orientation of the axis of variation, and lives in a half-plane, while the anti-monogenic signal lives in the second (other) half-plane. Calculating the partial HT [44] in the correct axes will yield a suitable representation also, but the advantage of using the monogenic signal is that the orientation is *retrieved* directly from the observed image without having to perform HTs at all values of θ (or having to estimate θ). We also define the quaternionic Fourier transform (QFT) in 2-D by [37] and [47, p. 192]:

$$\begin{aligned} G_Q(\mathbf{q}) &= \mathcal{F}_{\mathcal{Q}}\left\{g\right\}(\mathbf{q}) \qquad (19)\\ &= \int_{\mathbb{R}^2} e^{-2\pi \boldsymbol{i} x_1 q_1} g(\mathbf{x}) e^{-2\pi \boldsymbol{j} x_2 q_2}\, d\mathbf{x}\\ g(\mathbf{x}) &= \mathcal{F}^{-1}_{\mathcal{Q}}\left\{G_Q\right\}(\mathbf{x})\\ &= \int_{\mathbb{R}^2} e^{2\pi \boldsymbol{i} x_1 q_1} G_Q(\mathbf{q}) e^{2\pi \boldsymbol{j} x_2 q_2}\, d\mathbf{x}. \qquad (20) \end{aligned}$$

The form in (19) is also suitable for quaternionic (i.e., not real-valued) signals $g(\mathbf{x})$, and this makes the appropriate left and right multiplication important. The QFT can recover separate parity structure in x_1 and x_2 as it separately records four real values at each quaternion frequency $\mathbf{q}$.

III. Quaternionic Wavelet Analysis

A. Quaternionic Wavelets

In 2-D the CWT of $g(\mathbf{x}) \in L^2(\mathbb{R}^2)$ requires choosing an admissible mother wavelet $\psi(\mathbf{x}) \in L^2(\mathbb{R}^2)$[48]. To be admissible, the mother wavelet function, or $\psi(\mathbf{x})$, must satisfy the two conditions of

$$\begin{aligned} &0 < c_\psi < \infty, \text{ where } c_\psi = (2\pi)^2 \int_{E_2} \frac{|\Psi(\mathbf{f})|^2}{f^2}\, d\mathbf{f}\\ &\int_{E_2} |\psi(\mathbf{x})|^2\, d\mathbf{x} = 1. \qquad (21) \end{aligned}$$

Thus, the mother wavelet is constrained to be both a spatially local function, and to be mainly supported over some range of frequencies not including the origin, i.e., the function is oscillatory. Without loss of generality, center the mother wavelet function in space to $\mathbf{x} = \mathbf{0}$, and assume that $\Psi(\mathbf{f})$ is maximum at $\mathbf{f} = \mathbf{f}_0 = f_0\,(\cos(\phi_0) \quad \sin(\phi_0))^T$. From $\psi(\mathbf{x})$, a family of functions $\{\psi_{\boldsymbol{\xi}}(\mathbf{x})\}$ is defined by $\psi_{\boldsymbol{\xi}}(\mathbf{x}) = \mathcal{D}_a R_\theta \mathcal{T}_{\mathbf{b}}\left\{\psi\right\}(\mathbf{x}) = U_{\boldsymbol{\xi}}\psi(\mathbf{x})$, with $\boldsymbol{\xi} = (a, \theta, \mathbf{b})^T$. The purpose of including θ in the decomposition is to identify local behavior not aligned with the observational axes. The wavelet coefficients of function $g(\mathbf{x})$, and the reconstruction from the transform, are given by

$$\begin{aligned} w_\psi(\boldsymbol{\xi}, g) &= \int_{-\infty}^{\infty}\int_{-\infty}^{\infty} g(\mathbf{x})\psi^*_{\boldsymbol{\xi}}(\mathbf{x})\, d\mathbf{x}\\ g(\mathbf{x}) &= \frac{1}{c_\psi}\int_{-\infty}^{\infty}\int_{-\infty}^{\infty}\int_0^{2\pi}\int_0^{\infty}\\ &\quad \cdot \frac{w_\psi(\boldsymbol{\xi}, g)\psi_{\boldsymbol{\xi}}(\mathbf{x})\, da d\theta d\mathbf{b}}{a^3}. \qquad (22) \end{aligned}$$

It is frequently easier to interpret the nonnegligible coefficients $\{w_\psi(\boldsymbol{\xi}, g)\}$, rather than trying to disentangle the full behavior of an image in the original spatial domain. For notational simplicity we shall write $w(\boldsymbol{\xi})$ for $w_\psi(\boldsymbol{\xi}, g)$, unless the ψ and g functions are of note. $\psi(\mathbf{x})$, the mother wavelet function, needs to be chosen with care so that $w(\boldsymbol{\xi})$ has suitable properties.

This article provides classes of wavelet functions so that the wavelet coefficients calculated are rotated monogenic signals in the index $\mathbf{b}$ at any fixed scale a. We (in general) use wavelets of the form

$$\psi(\mathbf{x}) = \psi^{(r)}(\mathbf{x}) + \boldsymbol{i}\psi^{(i)}(\mathbf{x}) + \boldsymbol{j}\psi^{(j)}(\mathbf{x}) + \boldsymbol{k}\psi^{(k)}(\mathbf{x}) \qquad (23)$$

where each $\psi^{(s)} \in L^2(\mathbb{R}^2)$ for $s = r,\ i,\ j,\ k$. Thus, for any fixed $\mathbf{x} \in \mathbb{R}^2$ it follows that $\psi(\mathbf{x}) \in \mathbb{H}$. Naturally the whole family of wavelet coefficients constructed from the family of wavelet functions must be constructed to enjoy suitable properties. An arbitrary member of the wavelet family is

$$\begin{aligned} \psi_{\boldsymbol{\xi}}(\mathbf{x}) = U_{\boldsymbol{\xi}}\,\psi(\mathbf{x}) &= \psi^{(r)}_{\boldsymbol{\xi}}(\mathbf{x}) + \boldsymbol{i}\psi^{(i)}_{\boldsymbol{\xi}}(\mathbf{x})\\ &\quad + \boldsymbol{j}\psi^{(j)}_{\boldsymbol{\xi}}(\mathbf{x}) + \boldsymbol{k}\psi^{(k)}_{\boldsymbol{\xi}}(\mathbf{x}). \qquad (24) \end{aligned}$$

The construction corresponds to individually translating, scaling and rotating the four components of the quaternionic function. We thus intend to construct the quaternionic wavelet family by first extending the real wavelet to a monogenic signal, and then scaling, rotating and shifting the monogenic mother wavelet. This family member will be a rotated monogenic signal. It is very important that the wavelet coefficients are interpretable, as they will be considered as a local projection of the image, and they, rather than any other given quantity, will be the basis for analysis. We shall demonstrate that the method we use to define the wavelet transform will endow the coefficients with suitable properties. Note that this distinction does not arise in 1-D as the act of analytization commutes with constructing the wavelet family, and so all the members of the analytic wavelet family with a positive choice of scale are analytic signals. Hypercomplex (another choice of a hyperanalytic signals with two auxiliary variables is the hypercomplex signal) wavelets do not in general give hypercomplex wavelet coefficients [18].

B. Monogenic Wavelets

The monogenic signal of a globally unidirectional signal could be represented as an Inverse UQFT (IUQFT) in $\boldsymbol{e}_\nu$, constructed only from the positive frequencies of the UQFT in $\boldsymbol{e}_\nu$, and had an interpretation from (17). The orientation of a unidirectional

signal could be determined directly by the ratio of the RT components. A scale-localized version of this construction would correspond to filtering the image in space and spatial frequency, thus isolating structure with a given period and spatial location, and then constructing the RTs of the local component. The route to constructing the scale localized monogenic signal in one step will be by using monogenic wavelet functions. The monogenic extension of any given real-valued mother wavelet $\psi^{(r)}(\mathbf{x})$ with admissibility constant c_r is given by

$$\begin{aligned}\psi^{+}(\mathbf{x}) &= \mathcal{M}\psi^{(r)}(\mathbf{x}) = \psi^{(r)}(\mathbf{x}) + \mathcal{R}\psi^{(r)}(\mathbf{x}) \\ &= \psi^{(r)}(\mathbf{x}) + \left(\boldsymbol{i}\,\psi^{(1)}(\mathbf{x}) + \boldsymbol{j}\,\psi^{(2)}(\mathbf{x})\right) \end{aligned} \tag{25}$$

where $\psi^{(1)} = \mathcal{R}_1\,\psi^{(r)}$, $\psi^{(2)} = \mathcal{R}_2\,\psi^{(r)}$. To satisfy the conditions of being a wavelet each function must be square integrable, and satisfy the admissibility condition, i.e., the two conditions of (21). First as

$$\begin{aligned}\int_{E_2} \psi^{(s)2}(\mathbf{x})\,d\mathbf{x} &= \int_{E_2} \left|\Psi^{(s)}(\mathbf{f})\right|^2 d\mathbf{f} \\ &\le \int_{E_2} \left|\Psi^{(r)}(\mathbf{f})\right|^2 d\mathbf{f} \\ &< \infty,\ s = 1, 2\end{aligned}$$

and so square integrability follows as the wavelets were constructed from a real mother wavelet. Denote by c_s the value of (21) with $\psi^{(s)}$. Equation (9) in combination with the fact that $\cos^2\phi$ and $\sin^2\phi$ are always between 0 and 1, imply that $0 < c_1 \le c_r < \infty$ and $0 < c_2 \le c_r < \infty$, unless $\psi^{(s)} \equiv 0$. $c_1 + c_2 = c_r$ so $\psi^{(1)}$ and $\psi^{(2)}$ cannot both be the zero function. Consequently $\psi^{(1)}$ and $\psi^{(2)}$ as the c_s are finite and nonzero for $s = 1, 2$, satisfy the admissibility condition (21), and are both wavelets or one of them is the zero function. The functions are not unit energy, but can easily be renormalized. We note that the monogenic extension of a real wavelet is also a wavelet, from the same arguments.

The monogenic wavelets may be represented in polar form via their moduli, orientations, and phases respectively given by using (13), this yielding $\left|\psi^{+}_{\boldsymbol{\xi}}(\mathbf{x})\right|$, $\nu_{\boldsymbol{\xi}}(\mathbf{x})$ and $\varphi_{\boldsymbol{\xi}}(\mathbf{x})$, respectively. The wavelet is a function with spatial energy given by the modulus square, has a local period given by $\varphi_{\boldsymbol{\xi}}(\mathbf{x})$, and is showing a "local orientation preference" to angle $\nu_{\boldsymbol{\xi}}(\mathbf{x})$. The MWT is decomposing the image in terms of localized oscillations with a local period determined from $\varphi_{\boldsymbol{\xi}}(\mathbf{x})$; see also the discussion in [36].

To understand the properties of the wavelet transform, we derive the form of the Fourier representations of the wavelets. The FT of the translated, dilated, and rotated monogenic wavelets is

$$\Psi^{+}_{\boldsymbol{\xi}}(\mathbf{f}) = \{1 + (-\boldsymbol{k}\cos(\phi-\theta) + \sin(\phi-\theta))\} \cdot \Psi^{(r)}_{\boldsymbol{\xi}}(\mathbf{f}). \tag{26}$$

Recall that θ is the rotation angle of the wavelet, and ϕ is the argument of the Fourier variable. The nature of the MWT may be deduced from (26): the frequencies are localized according to $\Psi^{(r)}_{\boldsymbol{\xi}}(\mathbf{f})$, with the extra directional selectivity afforded by $\cos(\phi - \theta)$ and $1 + \sin(\phi - \theta)$. We can note directly from this expression and (10) that the members of the family given by (24) generated from the monogenic wavelet $\psi^{+}(\cdot)$ are rotated monogenic signals.

1) Monogenic Isotropic Wavelets: If $\psi^{(r)}(\mathbf{x}) = \psi^{(e)}(x)$ is an isotropic mother wavelet function, then any member of the monogenic wavelet family in the Fourier domain is (with $\boldsymbol{\xi}_0 = (a, 0; \mathbf{b})^T$) given by

$$\begin{aligned}\psi^{+}_{\boldsymbol{\xi}}(\mathbf{x}) &= \psi^{(e)}_{\boldsymbol{\xi}_0}(\mathbf{x}) + \boldsymbol{i}\left(\cos(\theta)\psi^{(1)}_{\boldsymbol{\xi}_0}(\mathbf{x}) + \sin(\theta)\psi^{(2)}_{\boldsymbol{\xi}_0}(\mathbf{x})\right) \\ &\quad + \boldsymbol{j}\left(-\sin(\theta)\psi^{(1)}_{\boldsymbol{\xi}_0}(\mathbf{x}) + \cos(\theta)\psi^{(2)}_{\boldsymbol{\xi}_0}(\mathbf{x})\right) \\ \Psi^{+}_{\boldsymbol{\xi}}(\mathbf{f}) &= \{1 + (-\boldsymbol{k}\cos(\phi-\theta) + \sin(\phi-\theta))\} \\ &\quad \cdot a\Psi^{(e)}(af)\, e^{-j2\pi\mathbf{fb}}. \end{aligned} \tag{27}$$

This follows by direct calculation. As an example of the monogenic isotropic wavelet; see Fig. 1. The isotropic structure of the magnitude is clear, while local variation in the monogenic wavelet over the x_1 and x_2 directions respectively may be determined from the pure quaternion part of the wavelet. When the monogenic mother has a radially symmetric real part, then the $\boldsymbol{\xi}_\pi$ monogenic wavelet coincides with the $\boldsymbol{\xi}$ anti-monogenic wavelet with $\boldsymbol{\xi}_\pi = (a, \theta + \pi; \mathbf{b})^T$, or $\psi^{+}_{\boldsymbol{\xi}_\pi}(\mathbf{x}) = \psi^{-}_{\boldsymbol{\xi}}(\mathbf{x})$; see (27). An example of a monogenic isotropic family are the monogenic Morse wavelets; see [17], with special members of the family considered also by Cnops [19] and Brackx and Sommen [49]. The isotropic wavelets are defined in the Fourier domain by $\Psi^{(e)}_{n;l,m}(f) = A'_{n;l,m}\,(2\pi f)^l\, e^{-(2\pi f)^m}\, \mathrm{L}_n^{c'}[2\,(2\pi f)^m]$, where $c' = (2l+2)/m - 1,\ m \ge 1,\ l > 0,\ l \ge m/2 - 1$, $A'_{n;l,m} = \sqrt{m\,2^{c'+1}\,\Gamma(1+n)/\Gamma(n+c'+1)}$, and $L^c_n(\cdot)$ is the generalized Laguerre polynomial [50, Sec. 8.97]. The monogenic extension of the nth order mother isotropic Morse wavelet is therefore

$$\begin{aligned}\psi^{+}_{n;l,m}(\mathbf{x}) &= \psi^{(e)}_{n;l,m}(\mathbf{x}) + (\boldsymbol{i}\,\cos\chi + \boldsymbol{j}\,\sin\chi) \\ &\quad \cdot 2\pi\left(\int_0^\infty df\; f\;\Psi^{(e)}_{n;l,m}(\mathbf{f})\; J_1(2\pi f x)\right) \end{aligned} \tag{28}$$

with $J_\nu(\cdot)$ a Bessel function of the first kind of order ν [50, p. 900]. Fig. 1 displays a plot of a monogenic isotropic Morse wavelet. The wavelets have isotropic support but recognize variation associated with the two spatial directions. Thus, the wavelets will localize signals in scale and represent the directional structure in the Riesz components.

2) Monogenic Directional Wavelets: In some applications, it may be suitable to localize signals in both scale and orientation, as several components are present at each position and at the same scale in different directions. Following work on discrete wavelet filters given in [1, p. 138] a real directional wavelet, based on the 1-D analytic continuous wavelet filters, will be constructed. Assume we have a 1-D analytic continuous wavelet function $\psi^{+}_{1D}(x_1) = \psi^{(e)}_{1D}(x_1) + \boldsymbol{j}\psi^{(o)}_{1D}(x_1)$, where $\psi^{(e)}_{1D}(x_1)$ is even, and $\psi^{(o)}_{1D}(x_1)$ is odd, where the FT of $\psi^{(\cdot)}_{1D}(x_1)$ is local to f_0. We define the $\pi/4$-directional wavelet by

$$\psi^{(\pi/4)}_{D}(\mathbf{x}) = \psi^{(e)}_{1D}(x_1)\psi^{(e)}_{1D}(x_2) - \psi^{(o)}_{1D}(x_1)\psi^{(o)}_{1D}(x_2). \tag{29}$$

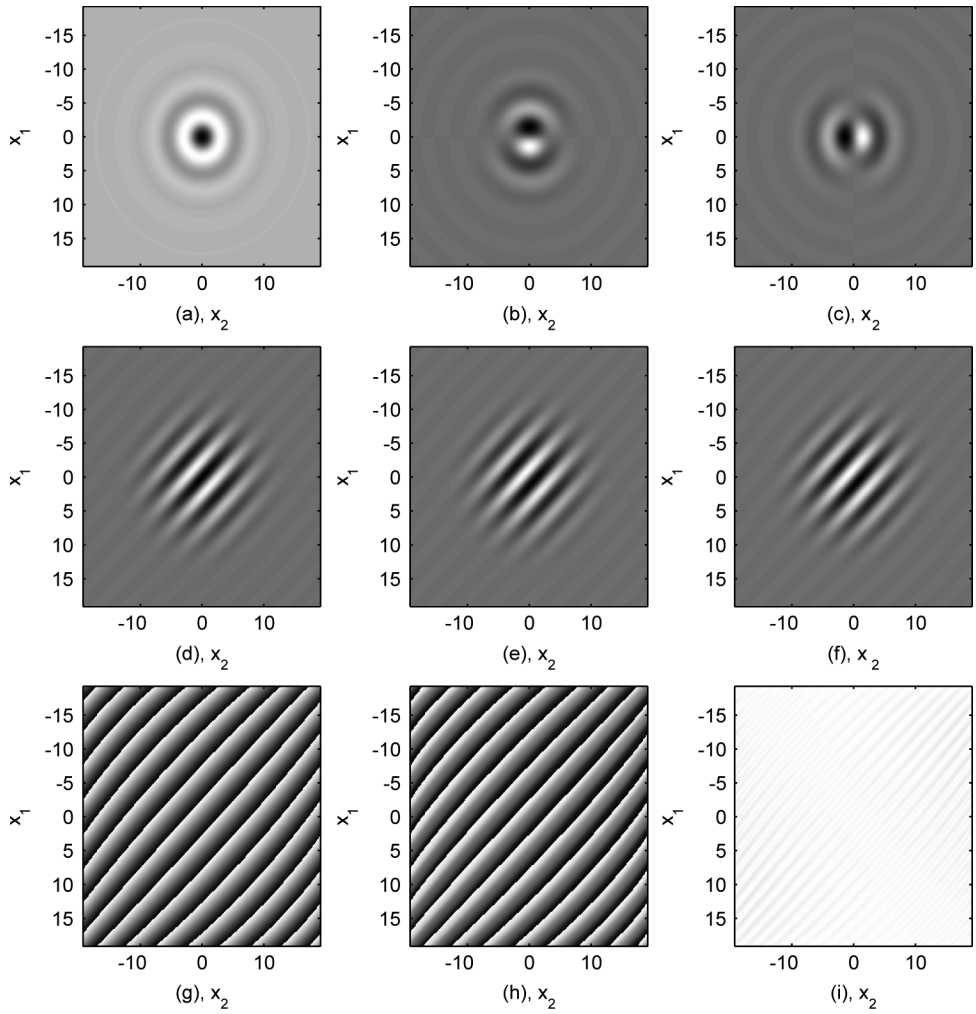

Fig. 1. The real part (a), and two imaginary parts, (b) and (c), of $\psi^{+}_{0;9,4}(\mathbf{x})$, $\psi_{D,0;9,4}(\mathbf{x})$ (d), and imaginary parts (e) $\psi^{(r)}_{D,0;9,4}(\mathbf{x})$ and (f) $\psi^{(h)}_{D,0;9,4}(\mathbf{x})$ of the monogenic directional Morse wavelet and the hypercomplex Morse wavelet respectively, with $n=0,\ \beta=9$ and $\gamma=4$, (g) the phase of $\psi^{++}_{D,0;9,4}$, (h) the phase of $\psi^{+}_{D,0;9,4}$ and (i) their absolute difference.

$\psi^{(\pi/4)}_D(\mathbf{x})$ is local in frequency to $\mathbf{f} = \pm\sqrt{2}f_0\,(\cos(\pi/4)\ \times\sin(\pi/4))^T$. To align the wavelet with the axis of observation we rotate the $\psi^{(\pi/4)}_D(\mathbf{x})$ function and define

$$\begin{aligned}\psi_D(\mathbf{x}) &= \psi^{(\pi/4)}_D(\mathbf{R}_{\pi/4}\mathbf{x})\\ &= \psi^{(e)}_{1D}\left(\frac{x_1-x_2}{\sqrt{2}}\right)\psi^{(e)}_{1D}\left(\frac{x_1+x_2}{\sqrt{2}}\right)\\ &\quad-\psi^{(o)}_{1D}\left(\frac{x_1-x_2}{\sqrt{2}}\right)\psi^{(o)}_{1D}\left(\frac{x_1+x_2}{\sqrt{2}}\right).\end{aligned}$$

$\Psi_D(\mathbf{x})$ will be local in frequency to $\mathbf{f} = \pm\sqrt{2}f_0\,(1\ 0)^T$. The RTs and partial HT [14] of the wavelet are

$$\begin{aligned}\psi^{(r)}_D(\mathbf{x}) &= \mathcal{R}_1\{\psi_D\}(\mathbf{x})\\ &= 4\int_0^\infty\int_0^\infty \frac{g_1+g_2}{\sqrt{2}g}\Psi^{(e)}(g_1)\\ &\quad\cdot\Psi^{(e)}(g_2)\sin\left(2\pi(\mathbf{R}_{-\pi/4}\mathbf{g})^T\mathbf{x}\right)\ d\mathbf{g}\\ \psi^{(h)}_D(\mathbf{x}) &= \mathcal{H}_1\{\psi_D\}(\mathbf{x}) = 4\int_0^\infty\int_0^\infty \Psi^{(e)}(g_1)\\ &\quad\cdot\Psi^{(e)}(g_2)\sin\left(2\pi(\mathbf{R}_{-\pi/4}\mathbf{g})^T\mathbf{x}\right)\ d\mathbf{g}\end{aligned}$$

$$\begin{aligned}&= \psi^{(o)}_{1D}\left(\frac{x_1-x_2}{\sqrt{2}}\right)\psi^{(e)}_{1D}\left(\frac{x_1+x_2}{\sqrt{2}}\right)\\ &\quad+\psi^{(e)}_{1D}\left(\frac{x_1-x_2}{\sqrt{2}}\right)\psi^{(o)}_{1D}\left(\frac{x_1+x_2}{\sqrt{2}}\right)\end{aligned}$$

$\mathcal{R}_2\{\psi_D\}(\mathbf{x}) \approx 0$ (see Appendix I). The complex[2] monogenic directional wavelet is formed by $\psi^{+}_D(\mathbf{x}) = \psi_D(\mathbf{x}) + \boldsymbol{i}\psi^{(r)}_D(\mathbf{x})$. We plot a real-valued directional wavelet in Fig. 1(d), and the Riesz component $\psi^{(r)}_D(\mathbf{x})$, in Fig. 1(e). We could also have constructed a complex-valued function by complementing $\psi_D(\mathbf{x})$ by using the partial HT [14] in x_1 operating on $\psi_D(\mathbf{x})$ to yield $\psi^{++}_D(\mathbf{x}) = \psi_D(\mathbf{x}) + \boldsymbol{i}\psi^{(h)}_D(\mathbf{x})$ (the hypercomplex wavelet or the dual tree $\mathbb{C}$-wavelet [1, p. 138]). Fig. 1(f) shows $\psi^{(h)}_D(\mathbf{x})$. When the Riesz component is constructed from $\psi_D(\mathbf{x})$, the spatial frequency modulation of $\Psi_D(\mathbf{f})$ is f_1/f rather than $\mathrm{sgn}(f_1)$, that would follow from using the partial HT. $\Psi_D(\mathbf{f})$ is mainly limited in frequency to $\mathbf{f} = \left(\pm\sqrt{2}f_0,\ 0\right)^T$, and for $\mathbf{f} = \left(\pm\sqrt{2}f_0 + \delta f_1,\ \delta f_2\right)^T$, $f_1/f = \pm 1 + \delta f_1/f_0^2 + o(\delta f_i^2)$,

[2]Formally $\psi^{+}_D(\mathbf{x}) = \psi_D(\mathbf{x}) + \boldsymbol{i}\psi^{(r)}_D(\mathbf{x})$, rather than $\psi_D(\mathbf{x}) + \boldsymbol{j}\psi^{(r)}_D(\mathbf{x})$, but any number system of the form of a real number plus a scaled pure unit quaternion is isomorphic to $\mathbb{C}$.

and so up to a small corrective error term $\psi_D^{(r)}(\mathbf{x}) = \psi_D^{(h)}(\mathbf{x})$. To investigate this, we plot the phases of the complex wavelets in Fig. 1(g) and 1(h), and their absolute difference (i). The difference in phases increases as we move away from $x_1 \approx -x_2$, but the amplitude of the wavelet will be simultaneously decreasing. The advantage of using directional wavelets is that they localize in direction. If the signal to be analysed has variability in several directions, i.e., is a 2-D signal, as defined by [51], then it will be well represented using directional wavelets if components of different orientation can be isolated using scale and orientation localization but not scale localization alone.

The advantage of using a second component constructed from the RT rather than the HT, i.e., using $\psi_D^{(r)}(\mathbf{x})$ rather than using $\psi_D^{(h)}(\mathbf{x})$, is that the quaternionic mother wavelet when rotated satisfies the relationships discussed in Section III-B, which will not (in general) be true for $\psi_D^{++}(x)$ [46, p. 58]. The complex-valued function $\psi_D^{+}(\mathbf{x})$ is a bona-fide monogenic function coupled with a single quaternionic conjugate, an anti-monogenic function. As a special choice of analytic wavelets to start from, we propose the usage of the Morse wavelets [16]. Directional wavelets have been previously constructed from 1-D Morse wavelets; see [48], but these are distinct wavelets.

IV. Quaternionic Wavelet Coefficients

A. The Quaternionic Wavelet Transform

Equation (22) defined the CWT coefficients of image $g(\mathbf{x})$ analysed with a wavelet family constructed from wavelet $\psi(\mathbf{x})$. If $\psi(\mathbf{x})$ is quaternionic then (22) takes the form

$$\begin{aligned} w(\boldsymbol{\xi}) &= \int_{-\infty}^{\infty}\int_{-\infty}^{\infty} g(\mathbf{x})\ (\psi_{\boldsymbol{\xi}}(\mathbf{x}))^*\ d\mathbf{x} \\ &= w^{(r)}(\boldsymbol{\xi}) - \boldsymbol{i}w^{(i)}(\boldsymbol{\xi}) - \boldsymbol{j}w^{(j)}(\boldsymbol{\xi}) - \boldsymbol{k}w^{(k)}(\boldsymbol{\xi}) \end{aligned} \quad (30)$$

thus defining $w^{(u)}(\boldsymbol{\xi}),\ \ u = r,\ i,\ j,\ k$. The local structure at $\boldsymbol{\xi}$ is given a four-vector valued representation, via some phase/s representations or relative magnitudes of the $w^{(u)}(\boldsymbol{\xi})$. "Local energy" is determined from the local magnitude square, $|w(\boldsymbol{\xi})|^2$, of the image $g(\mathbf{x})$. Define $\boldsymbol{\zeta} = (a, \theta, \mathbf{f}_b)^T$, where $\mathbf{f}_b$ is the Fourier variable after the Fourier transform in $\boldsymbol{b}$ has been implemented, and $\boldsymbol{\kappa} = (a, \theta, \boldsymbol{q}_b)^T$, where $\boldsymbol{q}_b$ is the QFT variable of $\boldsymbol{b}$. The local energy of $g(\mathbf{x})$ at $\boldsymbol{\xi}$ is defined by the scalogram of $g(\mathbf{x})$ given by

$$\begin{aligned} S(\boldsymbol{\xi}) = |w(\boldsymbol{\xi})|^2 = w^{(r)2}(\boldsymbol{\xi}) + w^{(i)2}(\boldsymbol{\xi}) \\ + w^{(j)2}(\boldsymbol{\xi}) + w^{(k)2}(\boldsymbol{\xi}). \end{aligned} \quad (31)$$

Irrespective of what quaternionic mother wavelet function is used, the magnitude square of the coefficients is interpreted as local signal presence at index $\boldsymbol{\xi}$. The interpretation is appropriate as the four wavelet functions $\psi^{(u)}(\mathbf{x})$ with $u = r,\ i,\ j,\ k$ will be chosen to be local to the *same position and wave-number*. See also [35, p. 1526] for a discussion of the time-frequency properties of RTs.

The relationships between the other components of the quaternionic wavelet will depend on the choice of mother wavelet function used to decompose the image, and so the phase representation of structure will vary with the mother wavelets used. To obtain coefficients with interpretable properties we calculate $w(\boldsymbol{\xi})$, so that it corresponds to a rotated monogenic signal in index $\mathbf{b}$ for any fixed value of θ and a. The signal $g(\cdot)$ could also be represented in terms of some weights attached with functions $\psi_{\boldsymbol{\xi}}(\cdot)$, that are monogenic in $\mathbf{x}$ for any fixed $\boldsymbol{\xi}_0$. In 1-D these two perspectives coincide, as analysis of a signal in terms of an analytic wavelet yields analytic wavelet coefficients and analytic wavelet functions. We introduce the additional notation of $\mathbf{J}_{\pi/2}\boldsymbol{\kappa} \equiv \left(a, \theta, \mathbf{J}_{\pi/2}\mathbf{q}_b\right)^T$. Note that $\mathbf{J}_{\pi/2}$ only operates on $\mathbf{q}_b$ in $\boldsymbol{\kappa}$.

Proposition 1: Forms of the FT and QFT of wavelet coefficients with real wavelet.

The FT and QFT of $w^{(r)}(\boldsymbol{\xi})$ for a real signal $g(\mathbf{x})$ with a real-valued wavelet $\psi^{(r)}(\cdot)$, respectively, are

$$W^{(r)}(\boldsymbol{\zeta}) = G(\mathbf{f}_b)\ a\Psi^{(r)*}(a\mathbf{R}_{-\theta}\mathbf{f}_b) \quad (32)$$

$$\begin{aligned} W_Q^{(r)}(\boldsymbol{\kappa}) &= \frac{1-\boldsymbol{k}}{2}\ G(\mathbf{q}_b)\ a\Psi^{(r)*}(a\mathbf{R}_{-\theta}\mathbf{q}_b) \\ &\quad + \frac{1+\boldsymbol{k}}{2}\ G(\mathbf{J}_{\pi/2}\mathbf{q}_b)\ a\Psi^{(r)*}(a\mathbf{R}_{-\theta}\mathbf{J}_{\pi/2}\mathbf{q}_b) \\ &= \frac{1-\boldsymbol{k}}{2}W^{(r)}(\boldsymbol{\kappa}) + \frac{1+\boldsymbol{k}}{2}W^{(r)}(\mathbf{J}_{\pi/2}\boldsymbol{\kappa}). \end{aligned} \quad (33)$$

Proof: Equations (32) and (33) follow by direct calculation, and are stated for comparison to the quaternionic wavelet coefficients. ∎

Proposition 2: Forms of the FT and QFT of wavelet coefficients with quaternionic wavelet.

The FT and QFT of $w(\boldsymbol{\xi})$ for a real signal $g(\mathbf{x})$ with a quaternionic wavelet $\psi(\cdot)$, respectively, are

$$\begin{aligned} W(\boldsymbol{\zeta}) = G(\mathbf{f}_b)\Big(&a\Psi^{(r)*}(a\mathbf{R}_{-\theta}\mathbf{f}_b) - \boldsymbol{i}a\Psi^{(i)*}(a\mathbf{R}_{-\theta}\mathbf{f}_b) \\ &- \boldsymbol{j}a\Psi^{(j)*}(a\mathbf{R}_{-\theta}\mathbf{f}_b) - \boldsymbol{k}a\Psi^{(k)*}(a\mathbf{R}_{-\theta}\mathbf{f}_b)\Big) \end{aligned}$$

$$\begin{aligned} W_Q(\boldsymbol{\kappa}) &= \frac{1}{2}W_\psi(\boldsymbol{\kappa}; g) - \frac{\boldsymbol{k}}{2}W_{\psi^{(r)} - \boldsymbol{i}\psi^{(i)} + \boldsymbol{j}\psi^{(j)} - \boldsymbol{k}\psi^{(k)}}(\boldsymbol{\kappa}; g) \\ &\quad + \frac{1}{2}W_\psi(\mathbf{J}_{\pi/2}\boldsymbol{\kappa}; g) \\ &\quad + \frac{\boldsymbol{k}}{2}W_{\psi^{(r)} - \boldsymbol{i}\psi^{(i)} + \boldsymbol{j}\psi^{(j)} - \boldsymbol{k}\psi^{(k)}}(\mathbf{J}_{\pi/2}\boldsymbol{\kappa}; g) \\ &\neq \frac{1-\boldsymbol{k}}{2}W_\psi(\boldsymbol{\kappa}; g) + \frac{1+\boldsymbol{k}}{2}W_\psi(\mathbf{J}_{\pi/2}\boldsymbol{\kappa}; g). \end{aligned} \quad (34)$$

Proof: See Appendix II-A. ∎

Equations (33) and (34) illustrate the new properties afforded by the quaternionic decomposition, in comparison to a real-valued decomposition of $g(\boldsymbol{x})$. The $\boldsymbol{i}$ and $\boldsymbol{k}$ coefficients will enable us to characterize structure in the x_1 axis, and we are not constrained to average the coefficients over x_1 and $-x_1$, as can be seen directly from (34). This enables us to recover phase-shifts, as otherwise we would average negative and positive shifts, as will be discussed.

The axes of observation are not necessarily aligned with the local axes of variation in the image. The CWT is covariant with respect to the transformation $\mathbf{x} \mapsto \mathbf{R}_{-\theta'}(\mathbf{x} - \mathbf{x}')$, i.e., if we observe $g(\mathbf{x}) = g_2(\mathbf{R}_{-\theta'}(\mathbf{x} - \mathbf{x}'))$, we may formally note that the transform takes the value $w(a, \theta - \theta', \mathbf{R}_{-\theta'}(\mathbf{b} - \mathbf{x}'); g_2(\mathbf{x}))$ [52, p. 40]. Having noted this equivariance of the CWT, one might assume that no discussion needs to be provided of changes of axes of observation. However, a discretization of

the calculation of the CWT, implies that we calculate the CWT coefficients at a *sampled* subset of all values of the locality index $\boldsymbol{\xi}$. Small misalignments in space between the wavelet function and the object under observation may cause the CWT coefficient at a given value of $\boldsymbol{\xi}$ to be small even if the signal has a large contribution at $\mathbf{x} = \mathbf{b}$ and $\mathbf{f} = a^{-1}\mathbf{R}_{-\theta}\mathbf{f}_0$. The down-sampling inherent in most filter bank implementations of the CWT exacerbates the spatial initialization problem. In 1-D, time shift variance has been considered in great detail; see also [3], [53], and the small misalignment in time may be considered in terms of shifts in phase. It is important that at any given $\boldsymbol{\xi}$ the transform of structure that corresponds to the same space and spatial frequency locality should not correspond to very different magnitudes due to small misalignments in space between the image and the wavelet. This becomes equivalent to requiring that the magnitude of the CWT does not change under phase-shifts of the signal.

B. The Monogenic Wavelet Transform

If at any given spatial point $g(\mathbf{x})$ corresponded to a single component, then the local characteristics of $g(\mathbf{x})$ could be extracted from $g^{\pm}(\mathbf{x})$, and the polar representation of (13) can be used directly to represent the signal. However, in general, $g(\mathbf{x})$ will correspond to a multiscale structure at the spatial point $\mathbf{x}$, and thus it is necessary to simultaneously implement a position and scale localization using (for example) a monogenic wavelet in order to produce interpretable polar representations of the signal.

In general, analysis with a monogenic but not necessarily monogenic isotropic mother wavelet, is implemented which takes the form $\psi(\cdot) = \psi^{+}(\cdot) = \psi^{(r)}(\cdot) + \boldsymbol{i}\psi^{(1)}(\cdot) + \boldsymbol{j}\psi^{(2)}(\cdot)$. A nonisotropic mother wavelet is a suitable choice when it is not reasonable to assume that the scale localization alone will be sufficient to separate components present in the image.

To interpret the MWT coefficients we shall show that the MWT annihilates the anti-monogenic component. This ensures that, equivalently, first the monogenic signal may be constructed and then scale localized; or first the image can be scale localized and then the monogenic extension of the local signal constructed. Indeed both operations can be implemented in one step using the MWT, and this then establishes the interpretation of the MWT coefficients. We write the MWT as $w^{+}(\boldsymbol{\xi})$, and note that the FT of the MWT of a real signal is given by

$$\begin{aligned} W^{+}(\boldsymbol{\zeta}) &= W^{(r)}(\boldsymbol{\zeta}) - \boldsymbol{i}W^{(1)}(\boldsymbol{\zeta}) - \boldsymbol{j}W^{(2)}(\boldsymbol{\zeta}) \\ &= \left(1 - \boldsymbol{k}\cos\left(\phi_b - \theta\right) + \sin\left(\phi_b - \theta\right)\right) W^{(r)}(\boldsymbol{\zeta}) \end{aligned}$$

recalling (5) and (34). From this equation the frequency domain properties of the monogenic wavelet coefficients can be determined. Note from (10) that we can immediately deduce that the MWT coefficients are rotated monogenic. If the real mother wavelet is radially symmetric, $\psi^{(r)}(\mathbf{x}) = \psi^{(e)}(x)$, then the rotation has no important effect in the definition of CWT, (30), as this assumption implies that $\Psi^{(e)}(f) \in \mathbb{R}$, and $a\Psi^{(e)*}(a\mathbf{R}_{-\theta}\mathbf{f}) = a\Psi^{(e)}(af)$. The FT of the MWT based on a real isotropic mother wavelet of a real signal is given by

$$\begin{aligned} W^{(e)}(\boldsymbol{\zeta}) &= \Psi^{(e)}(af_b)G(\mathbf{f}_b) \\ W^{+}(\boldsymbol{\zeta}) &= \left(1 + \left(-\boldsymbol{k}\,\cos(\phi_b - \theta) + \sin(\phi_b - \theta)\right)\right) \\ &\quad \Psi^{(e)}(af_b)G(\mathbf{f}_b) \\ &= \Psi^{+}(a\mathbf{R}_{-\theta}\mathbf{f}_b)G(\mathbf{f}_b) \neq \Psi^{(+)*}(a\mathbf{R}_{-\theta}\mathbf{f}_b)G(\mathbf{f}_b) \\ &= \left(1 + \left(-\boldsymbol{k}\,\cos(\phi_b - \theta) + \sin(\phi_b - \theta)\right)\right) W_{\psi}^{(e)}(\boldsymbol{\zeta}; g). \end{aligned}$$

This relation will enable us to consider the properties of the magnitude of the wavelet coefficients under rotation. The FT of the MWT of a monogenic extension of a real signal takes the form

$$\begin{aligned} W^{\pm}(\boldsymbol{\zeta}; g^{+}) = \Big(&\left(1 \pm \cos(\theta)\right) G^{+}(\mathbf{f}_b) \\ &\pm \boldsymbol{k}\sin(\theta) G^{-}(\mathbf{f}_b)\Big) a\Psi^{(r)*}\left(a\mathbf{R}_{-\theta}\mathbf{f}_b\right). \end{aligned} \tag{35}$$

The anti-monogenic extension has an analogue form with the $\pm$ on the right-hand side replaced by $\mp$. To prove this result see Appendix II-B and set $\theta' = 0$. To be able to establish the interpretation of the MWT we need to consider if the monogenic wavelets annihilate elements of the monogenic decomposition.

Theorem 1: CWT of the rotated monogenic and anti-monogenic decomposition components. The Fourier transform of the MWT of the rotated monogenic and anti-monogenic extension of a real signal take the forms

$$\begin{aligned} W^{+}(\boldsymbol{\zeta}; \widetilde{g}^{+}_{-\theta,\theta}) &= \{2 + 2\sin(\phi_b - \theta) - 2\boldsymbol{k}\cos(\phi_b - \theta)\} W^{(r)}(\boldsymbol{\zeta}; g) \\ &= 2\widetilde{G}^{+}_{-\theta,\theta}(\mathbf{f}_b) a\Psi^{(r)*}(a\mathbf{R}_{-\theta}\mathbf{f}_b) \\ &= 2W^{(r)}(\boldsymbol{\zeta}; \widetilde{g}^{+}_{-\theta,\theta}) \\ W^{+}(\boldsymbol{\zeta}; \widetilde{g}^{-}_{-\theta\theta}) &= 0 \\ w^{+}(\boldsymbol{\xi}; \widetilde{g}^{+}_{-\theta,\theta}) &= 2w^{(r)}(\boldsymbol{\xi}; \widetilde{g}^{+}_{-\theta,\theta}),\ w^{+}(\boldsymbol{\xi}; \widetilde{g}^{-}_{-\theta\theta}) = 0. \end{aligned} \tag{36}$$

The MWT thus annihilates the rotated anti-monogenic image and the anti-monogenic CWT annihilates the rotated monogenic image: $W^{\pm}(\boldsymbol{\zeta}; g) = 1/2\ W^{\pm}(\boldsymbol{\zeta}; \widetilde{g}^{\pm}_{-\theta,\theta})$, $w^{\pm}(\boldsymbol{\xi}; g) = 1/2\ w^{\pm}(\boldsymbol{\xi}; \widetilde{g}^{\pm}_{-\theta,\theta})$. For any other angle than $\theta \pm l\pi, l \in \mathbb{Z}$, $w^{\pm}(\boldsymbol{\xi}; g)$ is a linear combination of $w^{\pm}(\boldsymbol{\xi}; g^{+}_{-\theta,\theta})$ and $w^{\pm}(\boldsymbol{\xi}; g^{-}_{-\theta,\theta})$. Furthermore if we assume $\psi^{(r)} = \psi^{(e)}$, with $\boldsymbol{\zeta}_{\pi} = (a, \theta + \pi, \boldsymbol{b})^{T}$:

$$\begin{aligned} W^{\pm}(\boldsymbol{\zeta}_{\pi}; g) &= \frac{1}{2}\, W^{\pm}(\boldsymbol{\zeta}_{\pi}; \widetilde{g}^{\mp}_{-\theta,\theta}) \\ w^{\pm}(\boldsymbol{\xi}_{\pi}; g) &= \frac{1}{2}\, w^{\pm}(\boldsymbol{\xi}_{\pi}; \widetilde{g}^{\mp}_{-\theta,\theta}). \end{aligned} \tag{37}$$

Proof: See Appendix II-B. ∎

Hence the MWT of a rotated monogenic signal observed in the rotated frame of reference, i.e., $\widetilde{g}^{+}_{-\theta,\theta}(\mathbf{x})$ is twice that of the real wavelet transform of the rotated monogenic signal $\widetilde{g}_{-\theta,\theta}(\mathbf{x})$. When analyzing a real signal, the MWT can be used to annihilate the anti-monogenic components in the real image, which is in complete analogy to the $d = 1$ analytic/anti-analytic case. Compare with (6.8) to (6.10), and in particular the unnumbered equation over (6.10), of [41]. These show that the AWT of an $d = 1$ real signal with respect to an analytic (anti-analytic) wavelet is equal to one half of the CWT of the analytic (anti-analytic) extension of the real signal with respect to the analytic (anti-analytic) wavelet. The relationships of Theorem 1 are thus generalizations of the unnumbered equation above

(6.10) of [41]. This implies that both in $d = 1$ and $d = 2$, the AWT or MWT of the real signal or image has the same phase and one half of the modulus of the CWT of the analytically or monogenically extended signal or image. This provides the interpretation of the local polar representation of the MWT.

Proposition 3: Construction of the local rotated monogenic signal.

The MWT of a real image $g(\mathbf{x})$ is equivalent to the scale localization of the rotated monogenic extension of the signal and the rotated monogenic extension of the scale-localized version of the image $g(\mathbf{x})$:

$$w^{+}(\boldsymbol{\xi};g) = \left(w^{(r)}(\boldsymbol{\xi}_0;\widetilde{g}_{-\theta})\right)_{\theta}^{+} = w^{(r)}(\boldsymbol{\xi};\widetilde{g}^{+}_{-\theta,\theta}). \tag{38}$$

Proof: See Appendix II-C. ∎

The left-hand side of (38) corresponds to the MWT of the real signal, while the middle equation is the rotated monogenic extension of the scale local signal $\widetilde{g}_{-\theta}(\mathbf{x})$, that corresponds to adding some suitable components to the real part of the CWT of $g(\mathbf{x})$. The right-hand side of (38) corresponds to first forming the monogenic extension of the signal, and then scale-localizing the extension to make the phase description of the signal interpretable. Thus, all three local descriptions, i.e., the MWT of a real signal, the real CWT of a rotated monogenic signal and the monogenic extension of a real CWT of a real-valued signal *may all therefore be viewed as equivalent*. The MWT can, assuming a single component has been retrieved at local index $\boldsymbol{\xi}$, be represented in polar form using (13) where the magnitude, phase and orientation are interpretable in terms of a local univariate variations and the rotated monogenic representation. Felsberg and Sommer discuss properties of the (distinct) monogenic scale-space in [25], which are related to some of the derived properties of the MWT. If we had chosen to define the MWT using $\tilde{R}_{\theta}$ rather than R_{θ} then establishing the equivalent of Proposition 3 is very simple: by using $\tilde{R}_{\theta}$ the orientation of the wavelet transform is relative to the global axes rather than the wavelet. We retain R_{θ} to keep consistency in the definition of the wavelet transform. If we may assume the signal corresponds to a local plane wave the following theorem specifies its representation.

Theorem 2: The MWT of a plane oscillatory signal.

The MWT of a single component separable oscillatory signal modelled by $c(\mathbf{x}) = a_c(\mathbf{x})\cos(2\pi\varphi_c(\mathbf{x}))$ where $a_c(\mathbf{x})$, as well as $\nabla\varphi_c(\mathbf{x})$ are assumed to be slowly varying, is

$$w^{+}(\boldsymbol{\xi};c) = a_c(\mathbf{b})a\left|\Psi^{(r)}(a\mathbf{R}_{-\theta}\boldsymbol{f}_c(\mathbf{b}))\right| e^{2\pi\boldsymbol{e}_{\mathbf{n}_c(\mathbf{b},\theta)}\left(\varphi_c(\mathbf{b})-\Phi_{\psi}(a\mathbf{R}_{-\theta}\boldsymbol{f}_c(\mathbf{b}))\right)} + o(1) \tag{39}$$

where $\boldsymbol{f}_c(\mathbf{x}) = \nabla\varphi_c(\mathbf{x}) = f_c(\mathbf{x})\left(\cos(\varphi_c(\mathbf{x}))\ \sin(\varphi_c(\mathbf{x}))\right)^T$, $\mathbf{n}_c^T(\mathbf{x},\theta) = (\cos(\varphi_c(\mathbf{x})-\theta)\ \sin(\varphi_c(\mathbf{x})-\theta))$, $\Psi^{(r)}(\mathbf{f}) = \left|\Psi^{(r)}(\mathbf{f})\right| e^{-2\pi\boldsymbol{j}\Phi_{\psi}(\mathbf{f})}$, and note that Hermitian symmetry imposes $\left|\Psi^{(r)}(\mathbf{f})\right| = \left|\Psi^{(r)}(-\mathbf{f})\right|$ as well as $\Phi_{\psi}(\mathbf{f}) = -\Phi_{\psi}(-\mathbf{f})$.

This result follows by direct calculation assuming $(a_c(\mathbf{x}), \nabla\varphi_c(\mathbf{x}))$ sufficiently slowly varying, and the $o(1)$ terms will be due to such variation over the width of the wavelet. Let $\mathbf{f}_0 = \arg_{f_1>0}\max\left|\Psi^{(r)}(\mathbf{f})\right|$. We note that a simplified description of the oscillatory signal $c(\mathbf{x})$ can be determined from the ridge of the CWT; see Gonnet and Torresani [54, p. 394] via the subspace of the locality index given by $\left\{\boldsymbol{\xi}:\ \boldsymbol{f}_c(\mathbf{b}) = a^{-1}\mathbf{R}_{\theta}\mathbf{f}_0\right\}$. Equation (39) can be used to characterize the oscillation at $\mathbf{x} = \mathbf{b}$ and if the signal would be more appropriately modelled as an aggregation of oscillatory signals as long as they are sufficiently separated, i.e., as long as the wavelet is sufficiently narrow in space and spatial frequency to separate the different component; see also [17] and [36], then the coefficients will still be interpretable. Using directional monogenic wavelets will allow us to analyze a larger class of signal as it is more reasonable to assume we can distinguish a collection of plane-waves if we localize in scale, position *and* orientation.

C. Phase-shifts for Unidirectional Variation

The stability of the CWT coefficients under given affine transformations of the argument is important. With the MWT we obtain suitable magnitude invariance for an arbitrary phase-shift, and in some instances obtain invariance under rotation. If the real mother wavelet is isotropic, then the MWT coefficients of a real image $g(\mathbf{x})$ at $\boldsymbol{\xi}$ will have a magnitude invariant to the value of θ. This implies that we are not sensitive to loss of magnitude due to local orientation misalignment. However, we would naturally like to also be able to *retrieve* the local orientation, from the MWT. A real signal $g(\mathbf{x})$ is considered as a 1-D directional at frequency $\mathbf{f}$ if $\exists\phi_0 \in (0,\pi)$ such that

$$G(\mathbf{f}) = \frac{\widetilde{G}(f)}{2}\left(\delta(\phi-\phi_0-\pi)+\delta(\phi-\phi_0)\right). \tag{40}$$

We shall in this article be analyzing real images: as $g(\mathbf{x}) \in \mathbb{R}$ its FT is Hermitian $G^{*}(\mathbf{f}) = G(-\mathbf{f})$, and thus necessitates having both a delta distribution component at ϕ_0 and $\phi_0 + \pi$.

Theorem 3: Directional selectivity of the MWT.

If the real mother wavelet is isotropic, and the analyzed signal $g(\mathbf{x})$ is directional over the support of the monogenic wavelet at $\boldsymbol{\xi}$ with directionality ϕ_0, then with $\boldsymbol{\xi}^{\dagger} = (a,\phi_0,\boldsymbol{b})^T$

$$\left|w^{(1)}\left(\boldsymbol{\xi}^{\dagger};g\right)\right|^2 = \left|w^{(1)}(\boldsymbol{\xi};g)\right|^2 + \left|w^{(2)}(\boldsymbol{\xi};g)\right|^2$$
$$\phi_0 - \theta = \tan^{-1}\left(\frac{w^{(2)}(\boldsymbol{\xi};g)}{w^{(1)}(\boldsymbol{\xi};g)}\right). \tag{41}$$

Proof: See Appendix II-D. ∎

Thus with an isotropic mother wavelet, the magnitude of the Riesz component wavelet coefficients is invariant to rotations, but is maximized in the first component if we rotate the wavelet to align with the directionality of the variations. Hence, we may determine the local directionality of the signal from the monogenic isotropic wavelet coefficients.

1) Phase-shifted Plane Wave Signals: For a plane wave present at a given point $\mathbf{x}$ we define the phase-shift operation on a signal $g(\mathbf{x})$ using the monogenic signal. Phase shifts could also have been defined in both the x_1 and x_2 axes using the hypercomplex signal [13].

Definition 5.1: Phase-shift of a plane wave.

For a real signal $g(\mathbf{x}) = \widetilde{g}_{-\theta}(\mathbf{R}_{-\theta}\mathbf{x})$ we note that the image may for any rotation angle θ be written in sinusoidal form and the phase-shifted by θ_s version of the signal is defined via

$$\begin{aligned}\Lambda_{\theta_s} g(\mathbf{x}) &\equiv \left|g^+(\mathbf{x})\right| \cos\left(2\pi\varphi(\mathbf{x}) - \theta_s\right) \\ &= \Re\left\{|g^+(\mathbf{x})| e^{2\pi\varphi(\mathbf{x})-\theta_s \underset{\nu}{\boldsymbol{e}}(\mathbf{x})}\right\} \\ &= \frac{1}{2}\left(e^{-\underset{\nu}{\boldsymbol{e}}(\mathbf{x})\theta_s}\widetilde{g}^+_{-\theta,\theta}(\mathbf{x}) + e^{\underset{\nu}{\boldsymbol{e}}(\mathbf{x})\theta_s}\widetilde{g}^-_{-\theta,\theta}(\mathbf{x})\right) \quad (42)\end{aligned}$$

where Λ_{θ_s} is the phase-shift operator.

Theorem 4: The MWT of the phase-shifted signal.

For a real signal $g(\mathbf{x})$ the rotated monogenic extension of the phase-shifted real image if $\widetilde{\nu}(\mathbf{x})$ is varying sufficiently slowly, i.e., assuming $\widetilde{\nu}(\mathbf{x}) = \widetilde{\nu}(\mathbf{x}_0)\ \forall \mathbf{x}$ such that $|g^+(\mathbf{x})|$ is on-negligible, takes the form

$$\begin{aligned}(\Lambda_{\theta_s} g)^+_\theta(\mathbf{x}) &= |g^+(\mathbf{x})| e^{\underset{\nu}{\boldsymbol{e}}(\mathbf{x})(2\pi\varphi(\mathbf{x})-\theta_s)} \\ &= e^{-\underset{\nu}{\boldsymbol{e}}(\mathbf{x})\theta_s}\widetilde{g}^+_{-\theta,\theta}(\mathbf{x}). \quad (43)\end{aligned}$$

The MWT of a phase-shifted signal, where the orientation of the signal is constant over the width of the wavelet is therefore given by

$$w^{\pm}(\boldsymbol{\xi}; \Lambda_{\theta_s} g) = e^{\mp \underset{\nu}{\boldsymbol{e}}(\boldsymbol{b})\theta_s} w^{\pm}(\boldsymbol{\xi}; g). \quad (44)$$

The magnitude of the MWT of a phase-shifted signal, when the local orientation of the signal is stable over the width of the wavelet, is equivalent to that of the non-phase-shifted signal.

Proof: See Appendix II-E. ∎

This implies that the phase-shift between two images that locally correspond to the same plane wave may easily be determined by (44), and the methods of [41] can be extended to this context (2-D) to extract common components across images which may be phase-shifted. The magnitude of the MWT is invariant to shifts of phase. This implies that there will be no migration of energy across scales, due to misalignment between the wavelet and the signal, which in turn shows the stability of the MWT to small spatial misalignment between the observed signal and the analysis filters.

V. Examples

One of the main advantages of the monogenic isotropic transform is to remove additional degrees of redundancy. If the scale localization is sufficient for localization and separation of components, then directional properties can be directly quantified in the monogenic representation via the orientation. We illustrate this by simulating a set of geometrically anisotropic random fields (see also [55]), and show their representation by both the monogenic directional wavelets and the monogenic isotropic wavelets. We apply the method of Eom [56] to simulate a long correlation (LC) random field. We define $\mathbf{G} = [\alpha\cos(\varsigma) \quad \sin(\varsigma); -\alpha\sin(\varsigma) \quad \cos(\varsigma)]$, with α specifying the degree of anisotropy, ς the orientation of anisotropy. The spectral density function [57, p. 58] of an LC field is defined in terms of $\boldsymbol{\omega}' = \mathbf{G}^{-1}\boldsymbol{\omega}$ by the equation shown at the bottom of the page. $\widetilde{\omega}$ specifies the periodicity of the field, d its rate of spatial decay, and ρ its overall magnitude. We simulate four random fields, each of size 128×128, where the sets of parameters are: $d = 0.49$, $\varsigma = 0$ and $\alpha = 4$ for all the four fields apart from the first where $\varsigma = \pi/2$, and i) $\widetilde{\omega} = 1.6$ and $\rho = 18$, ii) $\widetilde{\omega} = 1.6$ and $\rho = 18$, iii) $\widetilde{\omega} = 0.1$, and $\rho = 15$, and iv) $\widetilde{\omega} = 0.5$ and $\rho = 25$. These four realizations are then joined into a inhomogeneous random field, by contiguous placement of the individual fields; see Fig. 2(a), and denoted $y_1(\mathbf{x})$, $x_1,\ x_2 = 1, \ldots, 256$. The field is directional and spatially heterogeneous. Using only the isotropic Morse wavelets [17] at scale $a = 0.83$ we plot the wavelet transform at all shifts (rotations are redundant when using an isotropic wavelet). The two high frequency components are isolated by the isotropic Morse wavelet. Using the MWT yields a scalogram of Fig. 2(c), which has removed the oscillation in the scalogram due to the wavelet and random field being "in phase" and "out of phase." The directional nature of the field can be determined by using the two RT components; see Fig. 2(g). Thus, we may easily characterize the local nature of the random field from the monogenic isotropic Morse wavelet transform, using the estimated orientation from the unit quaternion of the MWT without localizing in orientation.

Using only the real part of a directional wavelet at scale $a = 1.22$ yields Fig. 2(d). Including the RT component to form the scalogram yields Fig. 2(e), and if we rotate the wavelet by $\pi/2$ we obtain Fig. 2(f). Again including the RT component removes the dependence of phase alignment between the wavelet and signal. We can with this representation characterize the local nature of the random field, and have isolated the directional nature, but in this case this will require sampling θ sufficiently finely to recover the nature of the field. To get a better feeling for the spatial localization of the two monogenic wavelets we plot their moduli in Fig. 2(h) and (i). The extra directional localization of the directional wavelets has been bought with spatial resolution, as is also clear from Fig. 2(c), (e), and (f), where the latter two are more "smeared out" than the isotropic transform in Fig. 2(c). It is clear from these Figures that both transforms are very useful to localize and characterize different components of the image.

The monogenic wavelet transform also permits the recovery of phase-shifted signals. We generate a random field and overlay a localized oscillatory function, as well as generate a random field and a phase-shifted version of the localized function. We generate the two signals by $y_2(\mathbf{x}) = J_0\left(0.44\pi x\right) e^{-(x/25)^2} +$

$$S(\boldsymbol{\omega}) = \rho\,|\alpha|^{-2}\left|3 - \frac{\widetilde{\omega}^2}{\alpha^2} - \cos\left(\omega'_1\right) - \cos\left(\omega'_2\right) - \cos\left(\omega'_1\right)\cos\left(\omega'_2\right)\right|^{-2d}.$$

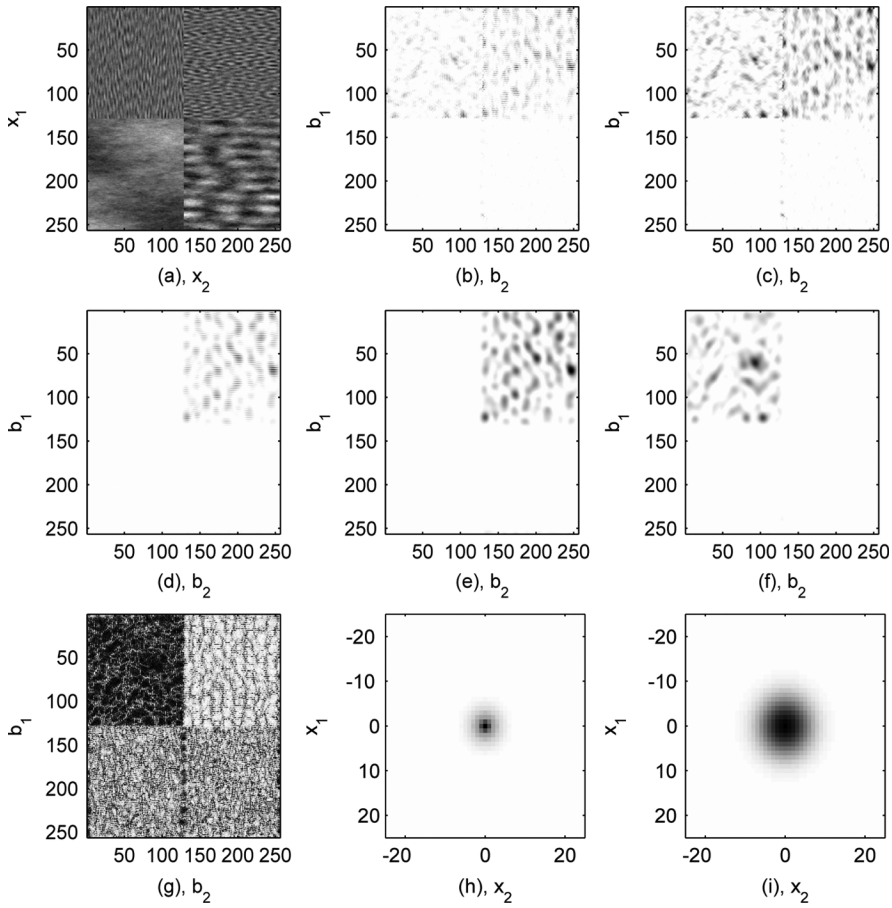

Fig. 2. A simulated random field (a), the magnitude square of the isotropic Morse wavelet coefficients (b), the magnitude square of the monogenic isotropic wavelet transform (c), the magnitude square of the directional real-valued wavelet transform of the field calculated at orientation 0 (d), the magnitude square of the directional monogenic wavelet transform of the field calculated at orientation 0 (e), calculated at orientation $\pi/2$ (f), the orientation of the monogenic isotropic wavelet transform of the field (g), the spatial magnitude of the monogenic isotropic wavelet (h), and the magnitude of the directional wavelet (i).

$\epsilon_1(\mathbf{x})$, and $y_3(\mathbf{x}) = J_0\left(0.44\pi x - \pi/3\right) e^{-x^2/25^2} + \epsilon_2(\mathbf{x})$, with $J_\nu(\cdot)$ a Bessel function of the first kind of order ν [50, p. 900], $\epsilon_k(\mathbf{x})$, $k = 1, 2$ are calculated as two independent realizations from a LC model with parameters $d = 0.49$, $\widetilde{\omega} = 0.1$, $\rho = 15$, $\alpha = 4.0$, $\varsigma = \pi/2$ and x_1, $x_2 = -128, \ldots, 127$. We calculate the monogenic transform of the original signal and extract the phase-shift using the phase of the monogenic signal, as well as the phase from the isotropic MWT at scale $a = 0.8259$. The phase-shift is found using Theorem 4. Comparing Fig. 3(a) and (b) shows the improved performance of the isotropic MWT to separate the structure of the windowed Bessel function from the directional "noise" signal. The phase-shift is estimated very near $\pi/3$ for a local region with $x_1 > 0$ (the phase-shift is $-\pi/3$ for $x_1 < 0$ due to our definition of the monogenic signal). As can be seen directly the estimate of the phase-shift between the two signals is much more accurate once the image has been scale localized. We also estimate the orientation of the Bessel function and this estimate also improves when using the localized signal [compare 3(c) with (d)]. The orientation is estimated using the triplet of transform coefficients, by comparing the two Riesz components of the transform; cf. (14). Note that $y_2(\mathbf{x})$ and $y_3(\mathbf{x})$ plotted in 3(e) and (f) are not strictly speaking 1-D signals in the sense of [51], but that the isotropic wavelets separate out the two different directional structures that spatially overlap.

VI. Conclusion

The MWT forms a natural 2-D extension of the AWT. Using the decomposition of a real-valued signal into a monogenic and an anti-monogenic signal helped to establish the equivalent interpretations of the transform as a rotated monogenic extension of local transform coefficients constructed from a real wavelet, or the real wavelet transform of the monogenic signal. This motivated the choice of definition of the MWT.

The monogenic signal gave us a natural framework for determining the properties of the MWT coefficients, and for establishing the interpretation of the local phase, orientation and amplitude of the signal defined from the MWT. If the signal is much more localized in orientation than the wavelet, then the local orientation calculated from the unit quaternion of the MWT will better represent the orientation of the variation in the signal, than the nominal orientation of the wavelet. The monogenic wavelets annihilate a component of the monogenic and anti-monogenic decomposition of a real-valued signal. This property allowed us to derive the local phase properties of the MWT coefficients. Phase shifts were defined using the monogenic signal. The MWT magnitude was shown to be invariant under shifts of phase and the MWT phase covariant, for given classes of signals. This established transform stability. When

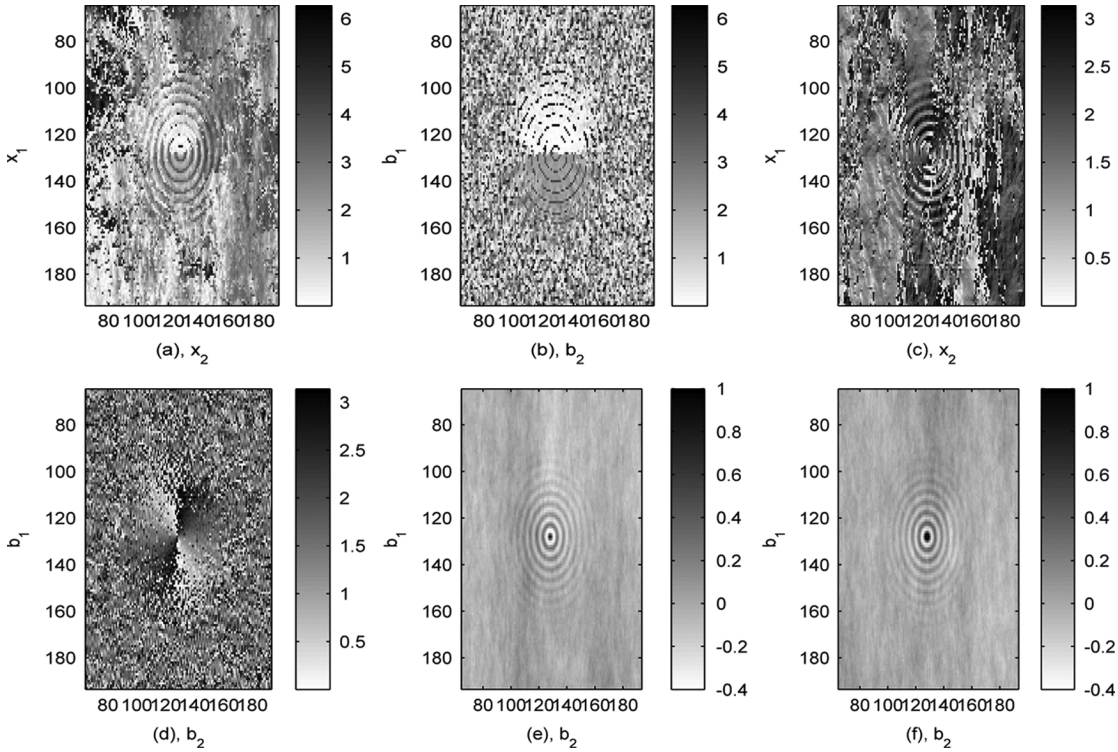

Fig. 3. Subplot (a) shows the difference between the estimated phase-shift and $\pi/3$ using the monogenic signal, while subplot (b) shows the difference between the estimated phase-shift and $\pi/3$ using the monogenic isotropic wavelet coefficients at scale $a = 0.8259$, (c) the estimated orientation of the pattern using the monogenic signal, (d) the estimated orientation of the pattern using the monogenic isotropic wavelet transform, (e) shows $y_2(\mathbf{x})$ and (f) $y_3(\mathbf{x})$.

using a monogenic isotropic wavelet to transform a unidirectional signal, the transform magnitude was shown to be invariant to rotations while the orientation was shown to be covariant to rotations. The orientation can be directly determined from the pure quaternion in the quaternionic representation of the transform. The wavelet ridges of a local plane wave were stated, and shown to possess a simple form.

Thus, this article defined the MWT to obtain interpretable transform coefficients, demonstrated the appropriateness of this definition, and showed the various suitable properties of the transform. Given these properties future application of the monogenic wavelet transform holds great promise, and appropriate discrete definitions [20] will further stimulate usage.

Appendix I
Properties of Monogenic Wavelets

We recall that $\Psi_{1D}^{(o)}(f) = -\boldsymbol{j}\Psi_{1D}^{(e)}(f)$, if $f > 0$, $\Psi_{1D}^{(o)}(f) = \boldsymbol{j}\Psi_{1D}^{(e)}(f)$, if $f < 0$. By calculating a FT of the rotated (29) we can write the 1-D real directional wavelet as

$$\begin{aligned}\psi_D(\mathbf{x}) = &\int_{-\infty}^{\infty}\int_{-\infty}^{\infty}\left(\Psi_{1D}^{(e)}\left(\frac{f_1-f_2}{\sqrt{2}}\right)\right.\\ &\cdot\Psi_{1D}^{(e)}\left(\frac{f_1+f_2}{\sqrt{2}}\right)-\Psi_{1D}^{(o)}\left(\frac{f_1-f_2}{\sqrt{2}}\right)\\ &\left.\cdot\Psi_{1D}^{(o)}\left(\frac{f_1+f_2}{\sqrt{2}}\right)\right)e^{2\boldsymbol{j}\pi\mathbf{f}^T\mathbf{x}}\,d\mathbf{f}\\ =&4\int_0^{\infty}\int_0^{\infty}\Psi_{1D}^{(e)}(g_1)\,\Psi_{1D}^{(e)}(g_2)\\ &\cdot\cos(2\pi\mathbf{g}^T\mathbf{R}_{\pi/4}\mathbf{x})\,d\mathbf{g}. \end{aligned}\tag{45}$$

Calculating a HT on the cosine in (45), we obtain

$$\begin{aligned}\psi_D^{(h)}(\mathbf{x}) = \mathcal{H}_1\left\{\psi_D^{(h)}(\mathbf{x})\right\} &= 4\int_0^{\infty}\int_0^{\infty}\Psi_{1D}^{(e)}(g_1)\\ &\cdot\Psi_{1D}^{(e)}(g_2)\sin(2\pi\mathbf{g}^T\mathbf{R}_{\pi/4}\mathbf{x})\,d\mathbf{g}\\ &=\frac{1}{2\boldsymbol{j}}\left(\psi^+\left(\frac{x_1-x_2}{\sqrt{2}}\right)\psi^+\left(\frac{x_1+x_2}{\sqrt{2}}\right)\right.\\ &\left.-\psi^-\left(\frac{x_1-x_2}{\sqrt{2}}\right)\psi^-\left(\frac{x_1+x_2}{\sqrt{2}}\right)\right)\\ &=\psi^{(e)}\left(\frac{x_1-x_2}{\sqrt{2}}\right)\psi^{(o)}\left(\frac{x_1+x_2}{\sqrt{2}}\right)\\ &+\psi^{(o)}\left(\frac{x_1-x_2}{\sqrt{2}}\right)\psi^{(e)}\left(\frac{x_1+x_2}{\sqrt{2}}\right).\end{aligned}\tag{46}$$

Direct calculation from (45) yields the result

$$\begin{aligned}&\psi_D^{(r)}(\mathbf{x})\\ &\quad=\mathcal{R}_1\{\psi_D\}(\mathbf{x}) = 4\int_0^{\infty}\int_0^{\infty}\Psi_{1D}^{(e)}(g_1)\\ &\quad\cdot\frac{g_1+g_2}{\sqrt{2}g}\Psi_{1D}^{(e)}(g_2)\sin(2\pi\mathbf{g}^T\mathbf{R}_{\pi/4}\mathbf{x})\,d\mathbf{g}\\ &\mathcal{R}_2\{\psi_D\}(\mathbf{x}) = 4\int_0^{\infty}\int_0^{\infty}\frac{-g_1+g_2}{\sqrt{2}g}\Psi_{1D}^{(e)}(g_1)\\ &\quad\cdot\Psi_{1D}^{(e)}(g_2)\sin(2\pi\mathbf{g}^T\mathbf{R}_{\pi/4}\mathbf{x})\,d\mathbf{g}\\ &\quad=8\int_0^{\infty}\int_0^{\sqrt{2}f_1}\frac{-f_2}{f}\Psi_{1D}^{(e)}\left(\frac{f_1-f_2}{\sqrt{2}}\right)\\ &\quad\cdot\Psi_{1D}^{(e)}\left(\frac{f_1+f_2}{\sqrt{2}}\right)\cos(2\pi(2x_1f_1))\\ &\quad\cdot\sin(2\pi(x_2f_2))\,d\mathbf{f}\approx 0\end{aligned}\tag{47, 48}$$

this result follows as the 1-D wavelet is only nonnegligible in $[f_0-\epsilon, f_0+\epsilon]$, for some small ϵ. The wavelet functions kill off contributions for values of f_2 that are not near zero, but if $f_2 \approx 0$ the integrand will be near zero from the sine function and Riesz kernel. Hence, the overall contribution from the second Riesz transform is negligible, and can be ignored (numerical computations verify this result).

Appendix II
Properties of the Quaternion WT

A. QFT of the Wavelet Coefficients With an Arbitrary Quaternionic Wavelet

The CWT with respect to a quaternionic wavelet is written in terms of its real components and we calculate the QFT component by component as follows:

$$\begin{aligned}
&\mathcal{F}_Q\{w(\boldsymbol{\xi})\}\\
&\quad=\mathcal{F}_Q\left\{w^{(r)}(\boldsymbol{\xi})\right\}-\boldsymbol{i}\mathcal{F}_Q\left\{w^{(i)}(\boldsymbol{\xi})\right\}\\
&\quad\quad-\mathcal{F}_Q\left\{w^{(j)}(\boldsymbol{\xi})\right\}\boldsymbol{j}-\boldsymbol{i}\mathcal{F}_Q\left\{w^{(k)}(\boldsymbol{\xi})\right\}\boldsymbol{j}\\
&\quad=\frac{1}{2}W_\psi(\boldsymbol{\kappa})-\frac{\boldsymbol{k}}{2}W_{\psi^{(r)}-\boldsymbol{i}\psi^{(i)}+\boldsymbol{j}\psi^{(j)}-\boldsymbol{k}\psi^{(k)}}(\boldsymbol{\kappa})\\
&\quad\quad+\frac{1}{2}W_\psi(\mathbf{J}_{\pi/2}\boldsymbol{\kappa})+\frac{\boldsymbol{k}}{2}W_{\psi^{(r)}-\boldsymbol{i}\psi^{(i)}+\boldsymbol{j}\psi^{(j)}-\boldsymbol{k}\psi^{(k)}}(\mathbf{J}_{\pi/2}\boldsymbol{\kappa})\\
&\quad\neq\frac{1-\boldsymbol{k}}{2}W_\psi(\boldsymbol{\kappa})+\frac{1+\boldsymbol{k}}{2}W_\psi(\mathbf{J}_{\pi/2}\boldsymbol{\kappa}).
\end{aligned}$$

B. Wavelet Transform of Rotated Monogenic and Anti-Monogenic Decomposition Components

By direct calculation, we find that

$$\begin{aligned}
&W^+(\boldsymbol{\zeta};\widetilde{g}^+_{-\theta',\theta'})\\
&\quad=W^+(\boldsymbol{\zeta};g)+\Big(\boldsymbol{i}\,W^+(\boldsymbol{\zeta};\widetilde{g}^{(1)}_{-\theta',\theta',R})\\
&\quad\quad+\boldsymbol{j}\,W^+(\boldsymbol{\zeta};\widetilde{g}^{(2)}_{-\theta',\theta',R})\Big)\\
&\quad=(1+\sin(\phi_b-\theta)+\cos(\phi_b-\theta)\cos(\phi_b-\theta')\\
&\quad\quad+\sin(\phi_b-\theta')+\sin(\phi_b-\theta)\sin(\phi_b-\theta')\\
&\quad\quad+\boldsymbol{k}(-\cos(\phi_b-\theta)-\cos(\phi_b-\theta')\\
&\quad\quad-\sin(\phi_b-\theta)\cos(\phi_b-\theta')+\cos(\phi_b-\theta)\\
&\quad\quad\cdot\sin(\phi_b-\theta')))\times W^{(r)}(\boldsymbol{\zeta};g). \qquad (49)
\end{aligned}$$

Therefore, it follows that

$$\begin{aligned}
&W^+_\psi(\boldsymbol{\zeta};\widetilde{g}^+_{-\theta,\theta})\\
&\quad=\{2+2\sin(\phi_b-\theta)-2\boldsymbol{k}\cos(\phi_b-\theta)\}\\
&\quad\quad\cdot W^{(r)}_\psi(\boldsymbol{\zeta};g)\\
&\quad=\{2+2\sin(\phi_b-\theta)-2\boldsymbol{k}\cos(\phi_b-\theta)\}\\
&\quad\quad\cdot G(\mathbf{f}_b)a\Psi^{(r)*}(a\mathbf{R}_{-\theta}\mathbf{f}_b)\\
&\quad=\{2+2\sin(\phi_b-\theta)-2\boldsymbol{k}\cos(\phi_b-\theta)\}\\
&\quad\quad\cdot\widetilde{G}_{-\theta,\theta}(\mathbf{f}_b)a\Psi^{(r)*}(a\mathbf{R}_{-\theta}\mathbf{f}_b)\\
&\quad=2\widetilde{G}^+_{-\theta,\theta}(\mathbf{f}_b)a\Psi^{(r)*}(a\mathbf{R}_{-\theta}\mathbf{f}_b)\\
&\quad=2W^{(r)}(\boldsymbol{\zeta};\widetilde{g}^+_{-\theta,\theta}). \qquad (50)
\end{aligned}$$

Furthermore *mutatis mutandis* with $\widetilde{g}^-_{-\theta,\theta}(\mathbf{x})$ replacing $\widetilde{g}^+_{-\theta,\theta}(\mathbf{x})$ we derive that $W^+_\psi(\zeta;\widetilde{g}^-_{-\theta,\theta})=0$. This completes the proof.

C. Construction of the Local Rotated Monogenic Signal

We note the form of the Fourier transform of $w^+_\psi(\boldsymbol{\xi};g)$ and then from (10) we find that

$$\begin{aligned}
&\mathcal{F}\left\{\left(w^{(r)}(\boldsymbol{\xi}_0;\widetilde{g}_{-\theta})\right)^+_\theta\right\}\\
&\quad=(1+\sin(\phi_b-\theta)-\boldsymbol{k}\cos(\phi_b-\theta))\\
&\quad\quad\cdot\widetilde{G}_{-\theta}(\mathbf{R}_{-\theta}\mathbf{f}_b)\,a\Psi^{(r)*}(a\mathbf{R}_{-\theta}\mathbf{f}_b)\\
&\quad=(1+\sin(\phi_b-\theta)-\boldsymbol{k}\cos(\phi_b-\theta))\,G(\mathbf{f}_b)\\
&\quad\quad\cdot a\Psi^{(r)*}(a\mathbf{R}_{-\theta}\mathbf{f}_b)\\
&\quad=W^+(\boldsymbol{\zeta};g).
\end{aligned}$$

Thus, $\left(w^{(r)}(\boldsymbol{\xi}_0;\widetilde{g}_{-\theta})\right)^+_\theta = w^+(\boldsymbol{\xi};g)$. For the second equality we start by taking $g(\mathbf{x})=1/2\left(\widetilde{g}^+_{-\theta',\theta'}(\mathbf{x})+\widetilde{g}^-_{-\theta',\theta'}(\mathbf{x})\right)$. By the linearity of the wavelet transform we have that with $\theta'=\theta$ using (50) and Appendix II-B:

$$\begin{aligned}
W^+(\boldsymbol{\zeta};g)&=\frac{1}{2}\left(W^+(\boldsymbol{\zeta};\widetilde{g}^+_{-\theta,\theta})+W^+(\boldsymbol{\zeta};\widetilde{g}^-_{-\theta,\theta})\right)\\
&=\frac{1}{2}\left(2W^{(r)}_\psi(\boldsymbol{\zeta};\widetilde{g}^+_{-\theta,\theta})+0\right)\\
&=W^{(r)}(\boldsymbol{\zeta};\widetilde{g}^+_{-\theta,\theta}).
\end{aligned}$$

D. Directional Selectivity

By direct calculation, we may note that

$$\begin{aligned}
&w^{(1)}(\boldsymbol{\xi})\\
&\quad=\int_{-\infty}^{\infty}\int_{-\infty}^{\infty}W^{(1)}(\boldsymbol{\zeta})e^{2\boldsymbol{j}\pi\mathbf{f}_b^T\mathbf{b}}\,d\mathbf{f}_b\\
&\quad\overset{(1)}{=}\int_0^{\infty}\int_0^{2\pi}(-\boldsymbol{j})f_b\cos(\phi_b-\theta)\frac{\widetilde{G}(f_b)}{2}\\
&\quad\quad\cdot(\delta(\phi_b-\phi_0-\pi)+\delta(\phi_b-\phi_0))\\
&\quad\quad\cdot a\Psi^{(e)}(af_b)e^{2\boldsymbol{j}\pi\mathbf{f}_b^T\mathbf{b}}\,df_b\,d\phi\\
&\quad=\cos(\theta-\phi_0)\int_0^{\infty}f_b\widetilde{G}(f_b)a\Psi^{(e)}(af)\\
&\quad\quad\cdot\sin\{2\pi f_b b\cos(\chi_b-\phi_0)\}\,df_b,\\
&w^{(2)}(\boldsymbol{\xi})\\
&\quad=\sin(\theta-\phi_0)\int_0^{\infty}f_b\widetilde{G}(f_b)a\Psi^{(e)}(af_b)\\
&\quad\quad\cdot\sin\{2\pi f_b b\cos(\chi_b-\phi_0)\}\,df_b.
\end{aligned}$$

For (1) to hold, we require $\psi^{(r)}(\mathbf{x})\equiv\psi^{(e)}(\mathbf{x})$, i.e., is isotropic, but if the rotation of the wavelet is small and $\Psi()$ is sufficiently smooth then the same result also follows. For a directional signal, when $w^{(1)}(\boldsymbol{\xi})\neq 0$, $\theta-\phi_0=\tan^{-1}\left(w^{(2)}(\boldsymbol{\xi})/w^{(1)}(\boldsymbol{\xi})\right)$. Also $w^{(2)}\left(\boldsymbol{\xi}^\dagger\right)=0$, and hence the result follows.

E. CWT of Phase-shifted Signal

If $\boldsymbol{e}_{\widetilde{\nu}}(\mathbf{x})=\boldsymbol{e}_{\widetilde{\nu}}$, across the width of the image, then as the Fourier transform corresponds to a right-hand multiplica-

tion, we may note $\mathcal{F}\left\{(\Lambda_{\theta_s} g^{+}_{-\theta,\theta}(\mathbf{x})\right\} = e^{-\boldsymbol{e}_{\nu}^{\sim}\theta_s}\widetilde{G}^{+}_{-\theta,\theta}(\mathbf{f})$. Refer to the wavelet transform of the phase-shifted signals as $w^{\pm}_{\theta_s}(\boldsymbol{\xi};g) = w^{\pm}(\boldsymbol{\xi};\Lambda_{\theta_s} g)$.

$$\begin{aligned}\Lambda_{\theta_s} g(\mathbf{x}) &= \left|g^{+}(\mathbf{x})\right| \cos\left(2\pi\varphi(\mathbf{x}) - \theta_s\right)\\ &= \frac{1}{2}\left(e^{-\boldsymbol{e}_{\nu}^{\sim}(\mathbf{x})\theta_s}\,\widetilde{g}^{+}_{-\theta,\theta}(\mathbf{x}) + e^{\boldsymbol{e}_{\nu}^{\sim}(\mathbf{x})\theta_s}\,\widetilde{g}^{-}_{-\theta,\theta}(\mathbf{x})\right).\end{aligned}$$

With the additional assumption that $\boldsymbol{e}_{\nu}^{\sim}(\mathbf{x}) = \boldsymbol{e}_{\nu}^{\sim}(\mathbf{b})$ is constant over the spatial width of the wavelet

$$\begin{aligned}w^{+}_{\theta_s}(\boldsymbol{\xi};g) &= \frac{1}{2}\left(w^{+}(\boldsymbol{\xi};e^{-\boldsymbol{e}_{\nu}^{\sim}(\mathbf{x})\theta_s}\,\widetilde{g}^{+}_{-\theta,\theta}(\mathbf{x}))\right.\\ &\quad \left.+w^{+}(\boldsymbol{\xi};e^{\boldsymbol{e}_{\nu}^{\sim}(\mathbf{x})\theta_s}\,\widetilde{g}^{-}_{-\theta,\theta}(\mathbf{x}))\right)\\ &= \frac{1}{2}\left(w^{+}(\boldsymbol{\xi};e^{-\boldsymbol{e}_{\nu}^{\sim}(\mathbf{b})\theta_s}\,\widetilde{g}^{+}_{-\theta,\theta}(\mathbf{x}))\right.\\ &\quad \left.+w^{+}(\boldsymbol{\xi};e^{\boldsymbol{e}_{\nu}^{\sim}(\mathbf{b})\theta_s}\,\widetilde{g}^{-}_{-\theta,\theta}(\mathbf{x}))\right)\\ &= \frac{1}{2}\left(e^{-\boldsymbol{e}_{\nu}^{\sim}(\mathbf{b})\theta_s} w^{+}(\boldsymbol{\xi};\,\widetilde{g}^{+}_{-\theta,\theta}(\mathbf{x}))\right.\\ &\quad \left.+e^{\boldsymbol{e}_{\nu}^{\sim}(\mathbf{b})\theta_s} w^{+}(\boldsymbol{\xi};\widetilde{g}^{-}_{-\theta,\theta}(\mathbf{x}))\right)\\ &= \frac{1}{2} e^{-\boldsymbol{e}_{\nu}^{\sim}(\mathbf{b})\theta_s} w^{+}(\boldsymbol{\xi};\,\widetilde{g}^{+}_{-\theta,\theta}(\mathbf{x}))\\ &= e^{-\boldsymbol{e}_{\nu}^{\sim}(\mathbf{b})\theta_s} w^{+}(\boldsymbol{\xi};g) \qquad (51)\end{aligned}$$

where we used Appendix II-B. Also from (50) we may note $w^{+}(\boldsymbol{\xi};g) = 1/2 w^{+}(\boldsymbol{\xi};\,\widetilde{g}^{+}_{-\theta,\theta})$, and thus the following result follows. From (44) we may note that $w^{\pm}_{\theta_s}(\boldsymbol{\xi};g) = e^{\mp \boldsymbol{e}_{\nu}(\boldsymbol{b})\theta_s} w^{\pm}(\boldsymbol{\xi};g)$, and thus it follows that $\left|w^{\pm}(\boldsymbol{\xi};\Lambda_{\theta_s} g)\right|^2 = \left|w^{\pm}(\boldsymbol{\xi};g)\right|^2$.

REFERENCES

[1] I. W. Selesnick, R. G. Baraniuk, and N. G. Kingsbury, "The dual-tree complex wavelet transform," *IEEE Signal Process. Mag.*, vol. 22, no. 6, pp. 123–51, 2005.

[2] E. P. Simoncelli, W. T. Freeman, E. H. Adelson, and D. J. Heeger, "Shiftable multiscale transforms," *IEEE Trans. Inf. Theory*, vol. 38, no. 2, pp. 587–607, Mar. 1992.

[3] R. A. Gopinath, "The phaselet transform—an integral redundancy near shift-invariant wavelet transform," *IEEE Trans. Signal Process.*, vol. 51, no. 7, pp. 1792–1805, Jul. 2003.

[4] F. C. A. Fernandes, R. L. C. van Spaendonck, and C. S. Burrus, "Multidimensional, mapping-based complex wavelet transforms," *IEEE Trans. Image Process.*, vol. 14, no. 1, p. 110, Jan. 2005.

[5] R. A. Scheper and A. Teolis, "Cramér-Rao bounds for wavelet transform-based instantaneous frequency estimation," *IEEE Trans. Signal Process.*, vol. 51, no. 6, pp. 1593–1603, Jun. 2003.

[6] C.-L. Tu, W.-L. Hwang, and J. Ho, "Analysis of singularities from modulus maxima of complex wavelets," *IEEE Trans. Inf. Theory*, vol. 51, no. 3, pp. 1049–1062, Mar. 2005.

[7] J. M. Lilly and S. C. Olhede, "Higher-order properties of analytic wavelets," *IEEE Trans. Signal Process.*, vol. 57, no. 1, pp. 146–160, Jan. 2009.

[8] J. M. Lilly and S. C. Olhede, "On the analytic wavelet transform," Imperial College Statistics Section, London, U.K., Tech. Rep. TR-07–02, 2007.

[9] A. C. Dixon, "On the Newtonian potential," *Quart. J. Math. Oxford Series*, vol. 35, pp. 283–96, 1904.

[10] R. J. Duffin, "Two-dimensional Hilbert transforms," *Proc. Amer. Math. Soc.*, vol. 8, pp. 239–45, 1957.

[11] M. Felsberg and G. Sommer, "The monogenic signal," *IEEE Trans. Signal Process.*, vol. 49, no. 12, pp. 3136–3144, Dec. 2001.

[12] S. L. Hahn and K. M. Snopek, "Wigner distributions and ambiguity functions of 2-d quaternionic and monogenic signals," *IEEE Trans. Signal Process.*, vol. 53, no. 8, pp. 3111–28, Aug. 2005.

[13] T. Bülow and G. Sommer, "Hypercomplex signals-a novel extension of the analytic signal to the multidimensional case," *IEEE Trans. Signal Process.*, vol. 49, no. 11, pp. 2844–2852, Nov. 2001.

[14] S. L. Hahn, *Hilbert Transforms in Signal Processing*. Norwood, MA: Artech House, 1996.

[15] M. Holschneider, *Wavelets: An Analysis Tool*. Oxford, U.K.: Oxford Univ. Press, 1995.

[16] S. C. Olhede and A. T. Walden, "Generalized Morse wavelets," *IEEE Trans. Signal Process.*, vol. 50, no. 11, pp. 2661–2670, Nov. 2002.

[17] G. Metikas and S. C. Olhede, "Multiple monogenic Morse wavelets," *IEEE Trans. Signal Process.*, vol. 55, no. 3, pp. 921–936, Mar. 2007.

[18] S. C. Olhede and G. Metikas, "The hyperanalytic wavelet transform," Statistics Section, Imperial College London, London, U.K., Tech. Rep. TR-06-02, 2006.

[19] J. Cnops, "The wavelet transform in Clifford analysis," *Comp. Methods Function Theory*, vol. 1, pp. 353–374, 2001.

[20] M. Unser, K. Balac, and D. V. D. Ville, "The monogenic Riesz-Laplace wavelet transform," presented at the 16h Eur. Signal Processing Conf., Lausanne, VD, Switzerland, 2008.

[21] F. Brackx, N. D. Schepper, and F. Sommen, "Clifford-Laguerre continuous wavelet transform," *Bull. Belgian Math. Soc.*, vol. 10, pp. 201–215, 2003.

[22] F. Brackx and F. Sommen, "The continuous wavelet transform in Clifford analysis," in *Clifford Analysis and its Application*, F. Brackx, J. Chisholm, and V. Soucek, Eds. Dordrecht, The Netherlands: Kluwer, 2001, pp. 9–26.

[23] W. L. Chan, H. Choi, and R. Baraniuk, "Directional hypercomplex wavelets for multidimensional signal analysis and processing," presented at the IEEE Int. Conf. Acoust., Speech, Signal Processing (ICASSP), Houston, TX, May 2004.

[24] T. A. Ell, "Hypercomplex Spectral Transformations," Ph.D. dissertation, Control Sciences and Dynamical System Dept., Univ. of Minnesota, Minneapolis, 1992.

[25] M. Felsberg and G. Sommer, "The monogenic scale-space: A unifying approach to phase-based image processing in scale-space," *J. Math. Imag. Vision*, vol. 21, p. 5, 2004.

[26] E. Bayro-Corrochano, "Multi-resolution image analysis using the quaternion wavelet transform," *Numer. Algorithms*, vol. 39, pp. 35–55, 2005.

[27] T. Bülow and G. Sommer, "Quaternionic Gabor filters for local structure classification," in *ICPR'98*, Brisbane, Australia, 1998, pp. 808–810.

[28] L. Traversoni, "Quaternion wavelets for moving volume representation," presented at the IEEE Int. Conf. Information Visualisation, IV, London, U.K., Jul. 2001.

[29] M. Miller and N. Kingsbury, "Image denoising using derotated complex wavelet coefficients," *IEEE Trans. Image Process.*, vol. 17, no. 9, pp. 1500–1511, Sep. 2008.

[30] M. Miller and N. Kingsbury, "Image modeling using interscale phase properties of complex wavelet coefficients," *IEEE Trans. Image Process.*, vol. 17, no. 9, pp. 1491–1499, Sep. 2008.

[31] C. C. Hsieh, "Motion smoothing using wavelets," *J. Intell. Robot. Syst.*, vol. 35, pp. 157–169, 2002.

[32] J.-X. He and B. Yu, "Wavelet analysis of quaternion-valued time-series ," *Int. J. Wavelets, Multires. Inf. Process.*, vol. 3, pp. 233–46, 2005.

[33] R. Duits, M. Felsberg, G. Granlund, and B. Romeny, "Image analysis and reconstruction using a wavelet transform constructed from a reducible representation of the euclidean motion group," *Int. J. Comp. Vision*, vol. 72, pp. 79–102, 2007.

[34] P. Cerejeiras, M. Ferreira, and U. Kähler, "Monogenic wavelets over the unit ball," *Zeitschrift für Analysis und ihre Anwendungen*, vol. 24, pp. 841–52, 2005.

[35] S. C. Olhede, "Hyperanalytic denoising," *IEEE Trans. Image Process.*, vol. 16, no. 6, pp. 1522–1537, Jun. 2007.

[36] G. Metikas and S. C. Olhede, "Wavelet coherence," in *Image Processing: Algorithms and Systems, Neural Networks, and Machine Learning, SPIE*, San Jose, CA, Jan. 2006, pp. 31–42.

[37] S.-C. Pei, J.-J. Ding, and J.-H. Chang, "Efficient implementation of quaternion Fourier transform, convolution, and correlation by 2-d complex FFT," *IEEE Trans. Signal Process.*, vol. 49, no. 11, pp. 2783–97, Nov. 2001.

[38] A. Sudbery, "Quaternionic analysis," *Math. Proc. Camb. Phil. Soc.*, vol. 85, pp. 199–225, 1979.

[39] L. Cohen, *Time-Frequency Analysis*. Englewood Cliffs, NJ: Prentice-Hall, 1995.

[40] M. A. Poletti, "The homomorphic analytic signal," *IEEE Trans. Signal Process.*, vol. 45, no. 8, pp. 1943–1953, Aug. 1997.

[41] S. C. Olhede and A. T. Walden, "Polarization phase relationships via multiple Morse wavelets—Part I: Fundamentals, Part II: Data analysis," *Proc. R. Soc. Lond. A*, vol. 459, p. 413, 2003.
[42] E. M. Stein and G. Weiss, *Fourier Analysis on Euclidean Spaces*. Princeton, NJ: Princeton Univ. Press, 1971.
[43] M. Felsberg, "Low-level image processing with the structure multivector," Ph.D. dissertation, Christian Albrechts Universität, Kiel, Germany, 2002.
[44] S. L. Hahn, "Multidimensional complex signals with single-orthant spectra," *Proc. IEEE*, vol. 80, p. 1287, 1992.
[45] S. C. Olhede and A. T. Walden, "Noise reduction in directional signals illustrated on quadrature doppler ultrasound," *IEEE Trans. Bio. Eng.*, vol. 50, pp. 51–57, 2003.
[46] E. M. Stein, *Singular Integrals and Differentiability Properties of Functions*. Princeton, NJ: Princeton Univ. Press, 1970.
[47] T. Bülow, M. Felsberg, and G. Sommer, "Non-commutative hypercomplex Fourier transforms of multidimensional signals," in *Geometric Computing with Clifford Algebras*, G. Sommer, Ed. Berlin, Germany: Springer, 2001, pp. 187–207.
[48] J.-P. Antoine, R. Murenzi, and P. Vandergheynst, "Directional wavelets revisited: Cauchy wavelets and symmetry detection in patterns," *Appl. Comput. Harmon. Anal.*, vol. 6, p. 314, 1999.
[49] F. Brackx and F. Sommen, "Clifford-Hermite wavelets in Euclidean space," *J. Fourier Anal. Appl.*, vol. 6, pp. 299–310, 2000.
[50] I. S. Gradshteyn and I. M. Ryzhik, *Table of Integrals, Series, and Products*, A. Jeffrey and D. Zwillinger, Eds., 6 ed. New York: Academic, 2000.
[51] G. Krieger and C. Zetzsche, "Nonlinear image operators for the evaluation of local intrinsic dimensionality," *IEEE Trans. Image Process.*, vol. 5, no. 6, pp. 1026–1042, Jun. 1996.
[52] J.-P. Antoine, R. Murenzi, P. Vandergheynst, and S. T. Ali, *Two-Dimensional Wavelets and their Relatives*. Cambridge, U.K.: Cambridge Univ. Press, 2004.
[53] R. R. Coifman and D. L. Donoho, "Translation-invariant denoising," in *Wavelets and Statistics (Lecture Notes in Statistics, Volume 103)*, A. Antoniadis and G. Oppenheim, Eds. New York: Springer-Verlag, 1995, pp. 125–50.
[54] C. Gonnet and B. Torresani, "Local frequency analysis with two-dimensional wavelet transform," *Signal Process.*, vol. 90, pp. 389–404, 1994.
[55] S. C. Olhede, "Localization of geometric anisotropy," *IEEE Trans. Signal Process.*, vol. 56, no. 5, pp. 2133–2138, May 2008.
[56] K. B. Eom, "Long correlation image models for textures with circular and elliptical correlation structures," *IEEE Trans. Image Process.*, vol. 10, no. 7, pp. 1047–1055, 2001.
[57] G. Christakos, *Random Field Models in Earth Sciences*. Mineola, New York: Dover, 1992.

Sofia C. Olhede was born in Spanga, Sweden, in 1977. She received the M. Sci. and Ph.D. degrees in mathematics from Imperial College London, London, U.K., in 2000 and 2003, respectively.

She held the posts of Lecturer from 2002 to 2006 and Senior Lecturer from 2006 to 2007 with the Mathematics Department, Imperial College London, and in 2007, she joined the Department of Statistical Science, University College London, where she is Professor of Statistics and Honorary Professor of Computer Science. Her research interests include the analysis of complex-valued stochastic processes, nonstationary time series, inhomogeneous random fields, and multiscale methods.

Prof. Olhede serves on the Research Section of the Royal Statistical Society, is a member of the Programme Committee of the International Centre for Mathematical Sciences, and is an Associate Editor of the *Journal of the Royal Statistical Society, Series B* (Statistical Methodology). She is a Fellow of the Royal Statistical Society and a member of the Institute of Mathematical Statistics, the London Mathematical Society, and the Society of Industrial and Applied Mathematics.

Georgios Metikas received the Ptychion degree from Aristotle University of Thessaloniki, Greece, in 1996 and the D.Phil. degree from Oxford University, Oxford, U.K., and 2000, respectively, both in theoretical physics.

He is currently with the Risk Analytics and Instruments Department at Deutsche Bank, London, U.K. His research interests are theoretical physics and image processing.